Facies (2007) 53: 1–26
DOI 10.1007/s10347-006-0090-0

ORIGINAL ARTICLE

Luke D. Nothdurft · Gregory E. Webb

Microstructure of common reef-building coral genera *Acropora*, *Pocillopora*, *Goniastrea* and *Porites*: constraints on spatial resolution in geochemical sampling

Received: 19 April 2006 / Accepted: 25 October 2006 / Published online: 5 December 2006

Abstract Scleractinian corals are increasingly used as recorders of modern and paleoclimates. The microstructure of four common reef-building coral genera is documented here: *Acropora*, *Pocillopora*, *Goniastrea*, and *Porites*. This study highlights the complexity and spatial variability of skeletal growth in different coral genera and suggests that a single growth model is too generalized to allow the accurate depiction of the variability observed in the four genera studied. New models must be introduced in order for coral skeletogenesis to be understood adequately to allow coral skeletons to serve as repositories of temporally constrained geochemical data. Owing to differences in microstructural patterns in different genera, direct observation of microstructural elements and growth lines may be necessary to allow microsamples to be placed into series that represent temporal sequences with known degrees of time averaging. Such data are critical for constraining microsampling strategies aimed at developing true time series geochemical data at very fine spatial and temporal scales.

Keywords Scleractinian corals · Microstructure · Paleoclimate · *Porites*

Introduction

The geochemistry of scleractinian coral skeletons is increasingly applied to the study of paleoclimate (e.g., Beck et al. 1992; de Villiers et al. 1995; Marshall and McCulloch 2002; McGregor and Gagan 2003), coastal run-off (e.g., Alibert et al. 2003; McCulloch et al. 2003), marine pollution (e.g., Fallon et al. 2002), ocean up-welling (Lea et al. 1989), and even marine productivity (Wyndham et al. 2004). Techniques such as laser ablation-inductively coupled plasma-mass spectrometry (LA-ICP-MS) (e.g., Sinclair et al. 1998; Fallon et al. 1999; McCulloch et al. 2003; Runnalls and Coleman 2003; Sinclair and McCulloch 2004), ion microprobe (Allison and Tudhope 1992; Allison 1996; Cohen et al. 2001, 2002; Meibom et al. 2003; Rollion-Bard et al. 2003) and vibrational spectroscopy (Cuif and Dauphin 1998; Cuif et al. 2003a) now allow sampling at increasingly fine levels of resolution with the hope of increased, even monthly or daily, temporal resolution (Cohen et al. 2001; Gill et al. 2006). However, for increased sampling resolution to reflect increased temporal resolution, a better understanding of patterns of coral skeletogenesis and resulting skeletal microstructure is required. Coral skeletal growth does not represent simple linear extension at microscopic scales (e.g., Sorauf 1972; Jell 1974; Cuif et al. 1997; Perrin 2003; Stolarski 2003). Thus, spatially sequential sample sets may not represent temporal sequences of coral growth capable of yielding true time series data. Additionally, all samples reflect some amount of time averaging, in extreme cases, over long time spans (e.g., more than 1 year).

The microstructure of coral skeletons has been studied for well over a century, but our understanding of coral biomineralization processes has improved particularly over the last 30 years. The 'spherulitic' hypothesis, or physio-chemical model of skeletal precipitation, based mostly on the work of Bryan and Hill (1941), has been replaced by more complex models wherein biomineralization is controlled by organic matrices (e.g., Goreau 1959; Towe 1972; Mitterer 1978; Johnston 1980; Constantz and Weiner 1988; Cuif et al. 1997; Gautret et al. 1997; Cuif and Sorauf 2001; Cuif et al. 2003a; Cuif and Dauphin 2005). The fundamental units of coral microstructure (i.e., fibers and centers of calcification) have been well established for many years, but Sorauf (1972) noted that fibers and centers of calcification are arranged differently in different scleractinian genera resulting in a variety of distinct three-dimensional microstructural patterns. The implications of those different patterns are still being elucidated (e.g., Roniewicz 1996; Cuif et al., 1997; Cuif and Perrin 1999; Perrin 2003; Stolarski 2003).

Current difficulties in interpreting coral skeletal geochemistry may be attributed partly to the failure to take

L. D. Nothdurft (✉) · G. E. Webb
School of Natural Resource Sciences, Queensland University of Technology,
GPO Box 2434, Brisbane QLD 4001, Australia
e-mail: l.nothdurft@qut.edu.au
Tel.: +61-7-38642198
Fax: +61-7-38641535

skeletal microstructure into account. For example, Sr/Ca thermometry in corals has been attempted at several temporal scales with correlation coefficients between Sr/Ca ratios and monthly sea-surface temperatures (SST) of better than 0.8 (Alibert and McCulloch 1997; Linsley et al. 2000). However, data tend to be noisy, and at least nine different Sr/Ca paleotemperature equations have been published for the genus *Porites* alone (e.g., a Sr/Ca value of 9 mmol/mol yields SST's ranging from 22.5 to 28°C; Cohen et al. 2002). Corrège (2006) calculated similar results in an up-to-date summary of published Sr/Ca vs SST calibrations for *Porites*. Some of the 'noise' in analyses may reflect vital effects wherein trace-element distributions correlate directly to microstructural patterns (e.g., Cohen et al. 2001; Marshall 2002; Rollion-Bard et al. 2003; Allison and Finch 2004; Meibom et al. 2004; 2006), but other noise could be produced by sampling non-sequential or inappropriately time-averaged data. Confidence in paleoclimate reconstruction requires a better understanding of all factors that may contribute to measured chemical signatures and to their spatial heterogeneity, and such understanding is particularly important as technology allows increasingly finer sampling resolutions.

The purpose of this paper is to document the microstructure of four important reef-building coral genera, including *Porites*, which is widely analyzed as a geochemical archive. Coral growth rates (i.e., rates of extension) are discussed in terms of specific skeletal microstructure in order to determine the range of temporal relationships possible between closely spaced skeletal elements. Such data are critical if we are to constrain microsampling strategies aimed at developing true time series geochemical data at very fine scales. Additionally, although the skeletal microstructure of extinct Paleozoic corals (Rugosa and Tabulata) has been studied extensively for taxonomic and phylogenetic analysis (Wang 1950; Kato 1963; Seminoff-tian-Chansky 1984; Lafuste and Plusquellec 1987; Rodriguez 1989; Oekentorp 2001), similar microstructural applications to scleractinian coral taxonomy, with a few exceptions (e.g., Roniewicz 1996; Sorauf 1996; Cuif et al. 1997; Perrin 2003), have not been pursued as vigorously, despite the need for such studies having been demonstrated decades before (Sorauf 1972; Jell 1974; Jell and Hill 1974). Recent attempts to link skeletal microstructure with molecular phylogenetic techniques (Cuif et al. 2003b; Stolarski 2003) have given only partial support for microstructure-based phylogenetic relationships within the Scleractinia, but Cuif and Perrin (1999) suggested that this may partly be the result of the numerous uncertainties concerning the exact microstructural patterns of the species upon which major taxa are based. Hence, a better differentiation of microstructural patterns in scleractinian corals will have important implications for phylogenetic analysis within the group.

Coral skeletal microstructure

Scleractinian coral polyps build exoskeletons of aragonite ($CaCO_3$) crystals formed beneath a layer of organic material secreted by cells in the basal ectoderm of the polyp (Sorauf 1972). Individual aragonite 'crystals' are precipitated in a 'hydro-organic gel' (Cuif et al. 2004; Cuif and Dauphin 2005) and are arranged into macroscopic skeletal elements, such as walls, septa and dissepiments as controlled by the distribution of the ectoderm and organic matrix molecules at nanometer scales of organization (Cuif and Sorauf 2001; Cuif and Dauphin 2005; Stolarski and Mazur 2005). The dominant microstructural units of the coral skeleton have long been recognized as 'fibers' or 'crystallites'. However, skeletal fibers are not simple crystals, but are composite biocrystals wherein organic compounds and mineral ions interact at a sub-micrometer to molecular scale, with growth at the tips of the fibers oriented towards the soft tissues of the polyp (Cuif et al. 1997; Cuif and Dauphin 2005; Stolarski and Mazur 2005). Etching techniques reveal the remains of a cyclic biomineralization process characterized by the presence of micrometer scale zonations or growth lines perpendicular to the direction of growth (Fig. 1A) that

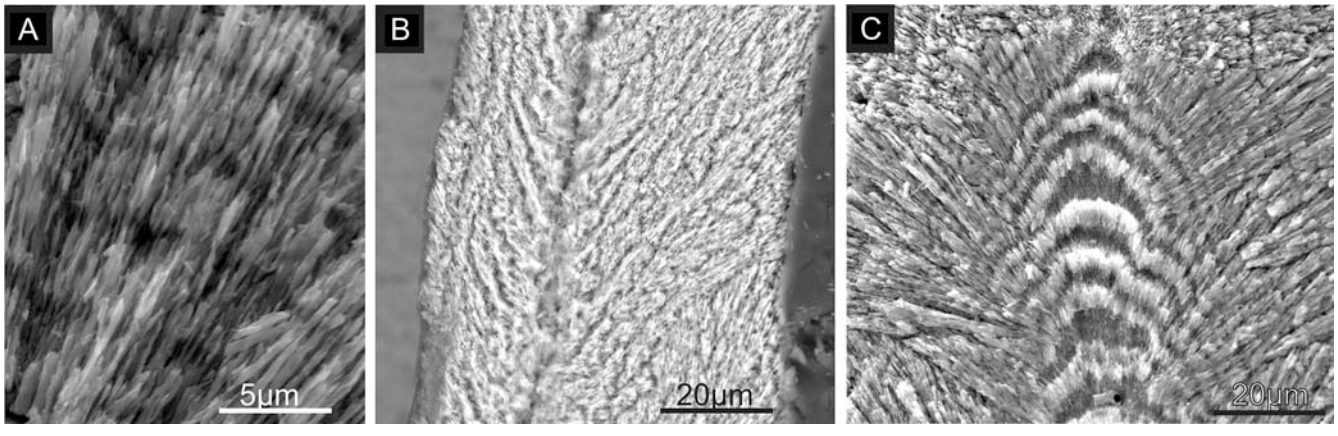

Fig. 1 Scanning electron photomicrographs of basic scleractinian coral skeletal microstructures on polished and etched sections. **A** Fibers with micrometer-scale zonation forming apparent growth increments perpendicular to the direction of growth; *Goniastrea favulus* (sample 98-6-12B). **B** Trabecula composed of skeletal fibers that radiate from the centers of calcification (*dark area*); *Pocillopora damicornis* (sample 03-10-92). **C** Layered growth of fibers and centers of calcification termed a 'center of rapid accretion' by Stolarski (2003); *Goniastrea favulus* (sample 04-9-30)

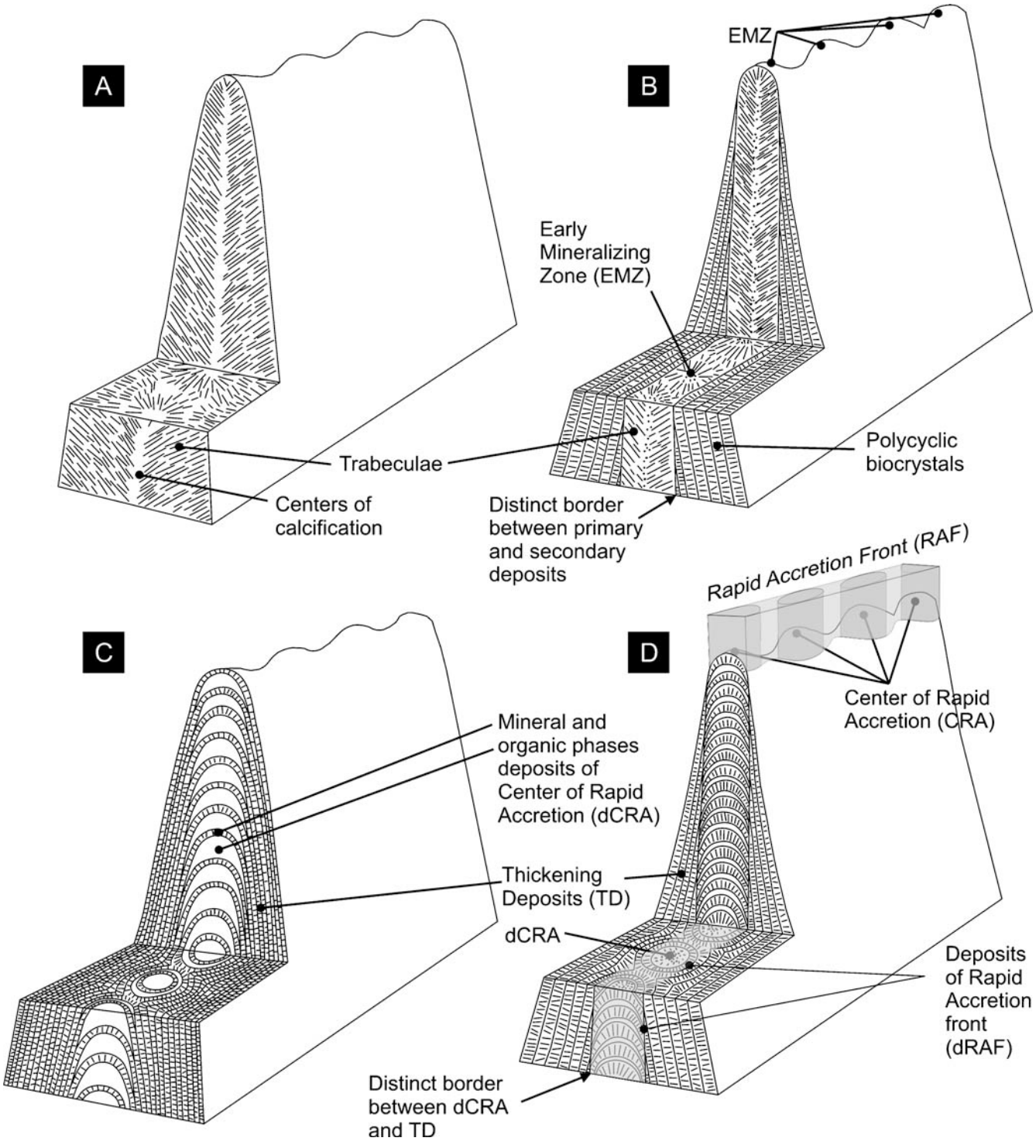

Fig. 2 Schematic diagrams of models of skeletal growth in scleractinian corals. **A** The 'spherulitic' or trabecular model of Bryan and Hill (1941) wherein distally directed trabeculae form adjacent cylinders that make up vertical skeletal elements. **B** The original 'two-step' model (Cuif et al. 1997) wherein the early mineralizing zone and trabeculae serve as scaffolding for fibrous layers that onlap as a secondary phase of skeleton growth with distinct discontinuity. **C**, **D** The two end members of the 'layered model' proposed by Stolarski (2003, his Fig. 17) here modified slightly to omit some detail. **C** End-member with continuous growth between 'Centers of Rapid Accretion' and thickening deposits. **D** End-member with a discontinuity between dCRA and TD, similar to Cuif's et al. (1997) two-step model (**B**)

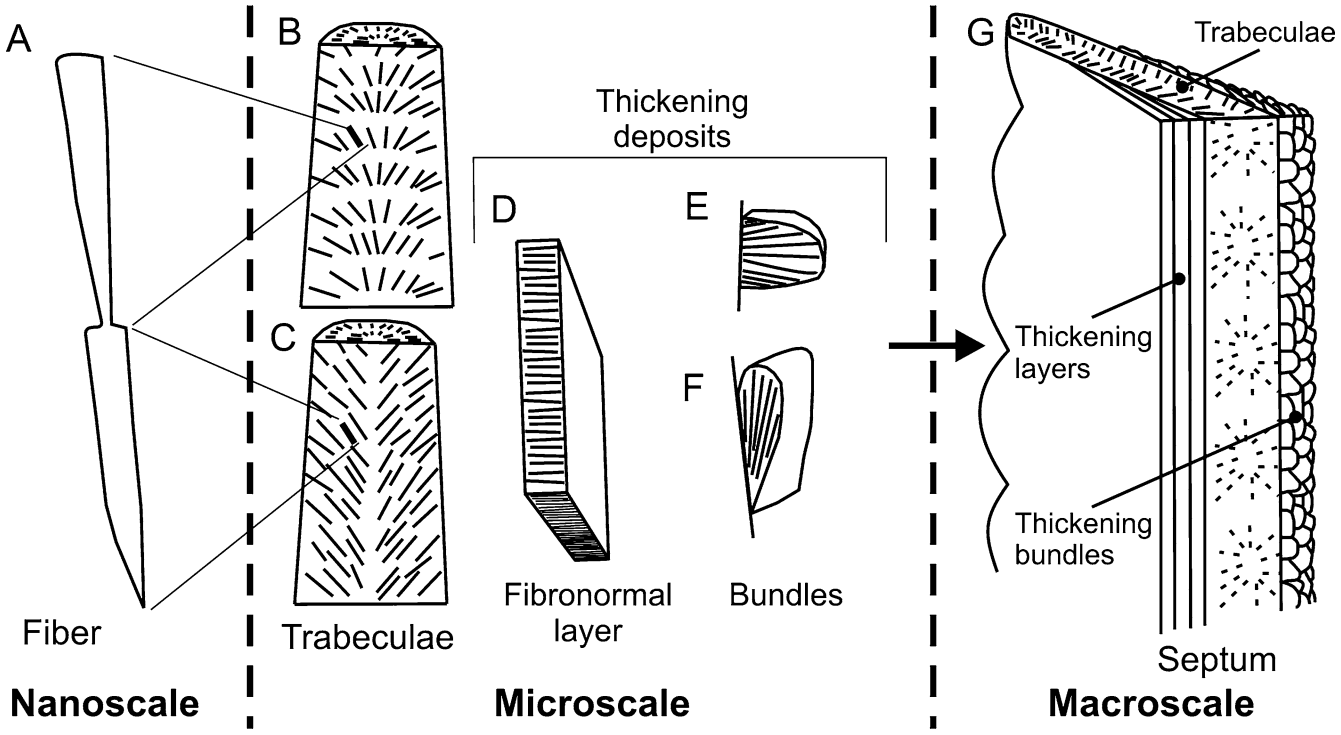

Fig. 3 Schematic diagram showing the three-dimensional spatial interplay between different microstructural associations of fibers that result in specific microstructural patterns in corals. **A** Individual fibers consist of alternating organic-rich and crystalline elements at nanoscales. Fibers are the dominant units of coral microstructure and are arranged into discrete geometric associations. These associations and their surface expressions are shown in **B**, **C**, **D**, **E** and **F. B** and **C** Trabeculae, both traditional and in the layered model of Stolarski (2003), result in spines or spinules at the surface. **D** Fibronormal layers typically result in smooth surfaces. **E**, **F** bundles result in smaller bumps on surfaces. **F** Bundles of subparallel to radiating fibers may lie at acute angles to the overall surfaces on which they are secreted thus forming shingles. **G** The various microstructural associations of fibers combine in three dimensions to form macroscopic skeletal structures such as septa. Thickening deposits on the trabeculae may be composed of either fibronormal layers or bundles

are thought to correspond to successive positions of the secretory ectoderm (e.g., Ogilvie 1896; Cuif and Sorauf 2001). Fluorescent staining techniques and atomic force microscopy suggest that the growth layers include intrafibrous organic components (Gautret et al. 2000; Cuif and Dauphin 2005). Thus, skeletal fibers with lengths of tens of micrometers consist of composite growth increments of aragonite approximately 3 to 5 μm long separated by thin organic-rich layers (Cuif and Sorauf 2001). Cuif and Dauphin (2005) showed that the increments are coordinated between adjacent microstructural elements.

Centers of calcification were differentiated as discrete structures by both microstructural and biochemical techniques by previous authors (e.g., Gautret et al. 1997). These centers were originally interpreted to contain micrometer-size, randomly orientated crystals at the centers of stacked radiating structures called trabeculae and were generally regarded as the areas where many individual fibers nucleate (Fig. 1B and 2A). However, in some cases, centers appear to consist primarily of organic matter with few preserved biocrystals (Stolarski 2003). The differences between centers of calcification and radiating fibers led to the development of a 'two-step model' of coral skeleton growth (Cuif et al. 1997), with the first phase of growth occurring in the organic-rich centers of calcification. The centers then served as scaffolding for successive growth of a distinctly separate, second phase of layers of aragonite fibers (Fig. 2B). The two steps highlight the temporal differences in the formation of distinct microstructural and biochemical units. The model was subsequently adjusted with calcification centers replaced by the 'early mineralization zone' (EMZ) (Cuif et al. 2003a).

Recently, Stolarski (2003) introduced a new model, the 'layered model', with new nomenclature to contrast with the traditional two-step model. In the layered model, centers of calcification are not fundamentally distinct from layers of fibers that cause skeletal thickening. Alternating layers of aragonite fibers and organic-rich zones pass through centers of calcification, suggesting the simultaneous formation of centers of calcification and lateral fibrous layers. However, Stolarski (2003) suggested two extreme end members. One depicts continuous growth of organi-mineral zones between 'centers of rapid accretion' (dCRA) (or EMZ sensu Cuif et al. 2003a) and 'thickening deposits' (TD) (or fibrous growth) with no disjunction between the two zones (Figs. 1C, 2C–D). The second extreme has a discontinuity between dCRA and TD due to an increased rate of growth at dCRA, which is similar to the original two step model of Cuif et al. (1997). Stolarski suggested that this boost in growth is mainly due to increased production of organic matrix and not mineral phases within the dCRA. As distribution of organic and mineral phases in the EMZ and in

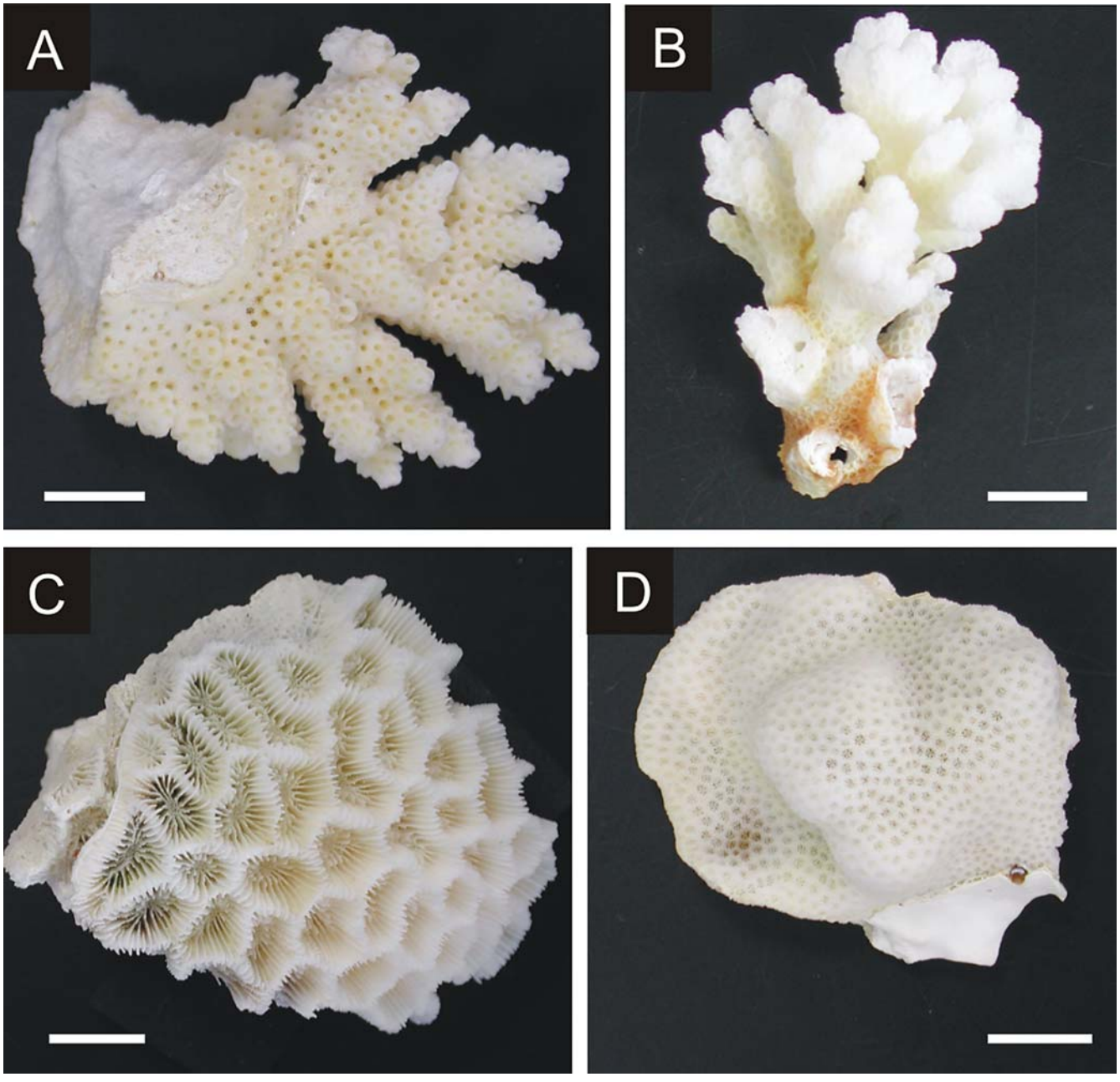

Fig. 4 The four common reef-building scleractinian coral species upon which the present study is based. **A** *Acropora hyacinthus* (sample 03-10-52). **B** *Pocillopora damicornis* (sample 03-10-70). **C** *Goniastrea favulus* (sample 04-9-30). **D** *Porites lobata* (sample 03-10-85). All samples were collected live from Heron Reef, Great Barrier Reef; *scale bars* are 1 cm

individual fibers has been better documented, the original two step model of Cuif et al. (1997) has evolved to encompass the cyclic alternation of organic-rich and mineral phases both in individual fibers and in the EMZ (Cuif and Dauphin 2005).

Irrespective of the models of skeletogenesis producing the specific micro- and nanostructures, it is the three-dimensional spatial-temporal interplay between different microstructural elements that provides specific microstructural patterns in corals. Different coral microstructures have been described in detail in some scleractinian genera since the advent of scanning electron microscopy, and the works of Sorauf (1972), Jell (1974), and Jell and Hill (1974) remain some of the best descriptions of microstructural relationships in coral skeletons. Sorauf (1972) and Roniewicz (1996) pointed out that fibers in corals occur in discrete geometric associations, and these associations combine in three dimensions to form macroscopic skeletal structures such as septa. The microstructural associations include: columns of radiating fibers (trabeculae), layers wherein parallel or palisaded fibers are perpendicular to the ectoderm (fibronormal microstructure), and bundles of subparallel to radiating fibers that may lie at low angles to the overall surfaces on which they are secreted (Fig. 3). The surface expression of

these microstructural elements varies between fibronormal layers typically resulting in smooth surfaces, trabeculae resulting in spines or spinules, and bundles resulting in smaller bumps commonly referred to as fasciculi (Wise 1970), tufts (Jell 1974), scales or shingles (Sorauf 1972). Much variability in microstructure between different coral genera is caused by differences in the occurrence and/or disposition of these microstructural fiber associations, and the focus of different researchers on genera that have different combinations of associations has contributed to some of the difficulties in interpreting scleractinian skeletogenesis. Additionally, much recent attention has been focused away from gross microstructure towards more nanostructural studies (i.e., of structure within individual fibers) (e.g., Cuif and Daupin 2005; Stolarski and Mazur 2005), and there has been a rapid evolution of microstructural concepts and terminology. However, with the illustration of very different microstructures in common corals such as *Fungia* (e.g., Sorauf 1972), *Acropora* (e.g., Gautret et al. 2000) and *Porites* (e.g., Cuif and Dauphin 2005), it is now clear that no single model of skeletal growth describes all genera equally. Thus, attention must focus on the relationship between different microstructural fiber associations (trabeculae, fibronormal layers and bundles) in order to establish the fine-scale temporal relationships within coral skeletons.

Methods and materials

For this study, four species of scleractinian coral, *Acropora hyacinthus*, *Pocillopora damicornis, Goniastrea favulus*, and *Porites lobata* (Fig. 4) were collected live from Heron Reef, an enclosed elongate lagoonal platform reef just south of the Tropic of Capricorn and 70 km from the mainland in the southern Great Barrier Reef, Australia. Fifteen specimens were collected of each species within 20 m of the reef margin. Samples were immersed in sodium hypochlorite (NaOCl) for 1–2 days to remove organic matter prior to analysis and rinsed thoroughly with deionized water. Portions of the samples were then set in epoxy resin.

Scanning electron microscope (SEM) observations were made using a FEI QUANTA 200 using several operation modes, including operation at high vacuum (15 and 20 kV) on samples coated with carbon and at 2–10 kV for uncoated samples using both secondary and backscattered electron images. Secondary electron images were recorded of freshly broken and external surfaces, with some specimens etched with dilute formic acid (2%) for 20 s prior to being carbon coated. Transverse and longitudinal ultrathin sections ('lame a faces polies' of Lafuste 1970) were prepared for observation using optical microscopy. Ultrathin sections are doubly polished thin sections that are 3–10 μm thick instead of the 30 μm of standard petrographic thin sections. Ultrathin sections have primarily been used for studying Paleozoic corals (e.g., Semenoff-tian Chansky 1984; Lafuste and Plusquellec 1985; Lafuste et al. 1993) but recently have also been used to study scleractinian corals (e.g., Perrin and Cuif 2001; Perrin 2003, 2004; Nothdurft and Webb in press). Ultrathin sections allow observation of fine-scale skeletal features and the crystallographic orientations of individual skeletal fibers.

Results

Acropora hyacinthus microstructure

Acropora hyacinthus forms vase- to plate-like colonies with branches primarily projecting horizontally. Fine upward-projecting branchlets 3–7 mm in diameter and up to 20 mm long extend from the branches (Wallace 1999). Each branchlet contains an axial corallite with 1–2 mm outer diameter, 0.4 to 1.1 mm inner diameter, and six primary septa. Radial corallites are evenly sized, adjoining and labellate (sensu Wallace 1999). The inner (towards the axial corallite) part of the wall of each corallite does not stand free and the outer walls extend outward around the branch forming a distinct rosette around the axial corallite (Fig. 5A–C). The depth of the calice (i.e., depth to the last dissepiment to form) is difficult to determine owing to the sparse and delicate nature of dissepiments. However, the best estimates are approximately 6 mm in radial corallites and up to 20 mm in axial corallites. Coenosteum is costate with spinules (small spines that occur in the coenosteum as opposed to within corallites). Spinule morphology is variable with irregular, rough-tipped spinules mainly on the underside of colonies and relatively smooth-tipped spinules on the upper side of the colony and on branchlets (Fig. 5D–F).

Fig. 5 Scanning electron photomicrographs of *Acropora hyacinthus*. **A** Distal view of a branchlet showing axial corallite (a) and smaller radial corallites (r) (sample 03-10-50). **B** Transverse section through a branchlet. Axial corallite is in center (a) with prominent septa. Radial corallites (r) surround the axial corallite and have costae (*white arrows*) that extend outward from the lip but no obvious septa (sample 03-10-16). **C** Lateral view of the outside of a radial corallite (r) on a branchlet. Costae (c) are ridge-shaped structures running up the outside of the radial corallite while spinules (s) are digitate structures covering coenostial areas of the branchlet (sample 03-10-50). **D** Lateral view of the outside of a radial corallite on a branchlet showing costae and spinules covered in shingle terminations. Shingles are better developed at the base of the corallite (sample 98-6-12C). **E** Spinules with smooth tips and synapticulae (*arrows*) at their base composed of shingles (sample 03-10-50). **F** Costae with predominantly smooth tips and interconnecting wall made of shingle microstructure developed from thickened synapticulae (sample 03-10-50). **G** Polished and etched surface with low-relief, overlapping shingle microstructure showing slight radiation of aragonite fibers within each bundle (sample 98-6-12C). **H** Polished and etched section of shingles viewed end on showing that the outermost edges of shingles are more resistant to acid etching than the inner aragonite fibers (sample 98-6-12C). **I**, **J** and **K** Polished and etched sections through trabecular microstructures that are surrounded by shingle microstructure. **I** Transverse section of area of trabecula and surrounding shingle development. The growth directions of the shingles are highly variable as indicated by the *black arrows*. *Crosses* indicate shingles that are directed in or out of the section (sample 03-10-44). **J** Prominent trabecula enveloped by shingle microstructure (sample WH-10). **K** Costae, indicated by *white arrows*, consisting of trabeculae with subsequent filling of intercostal space by shingle microstructure (sample 03-10-44)

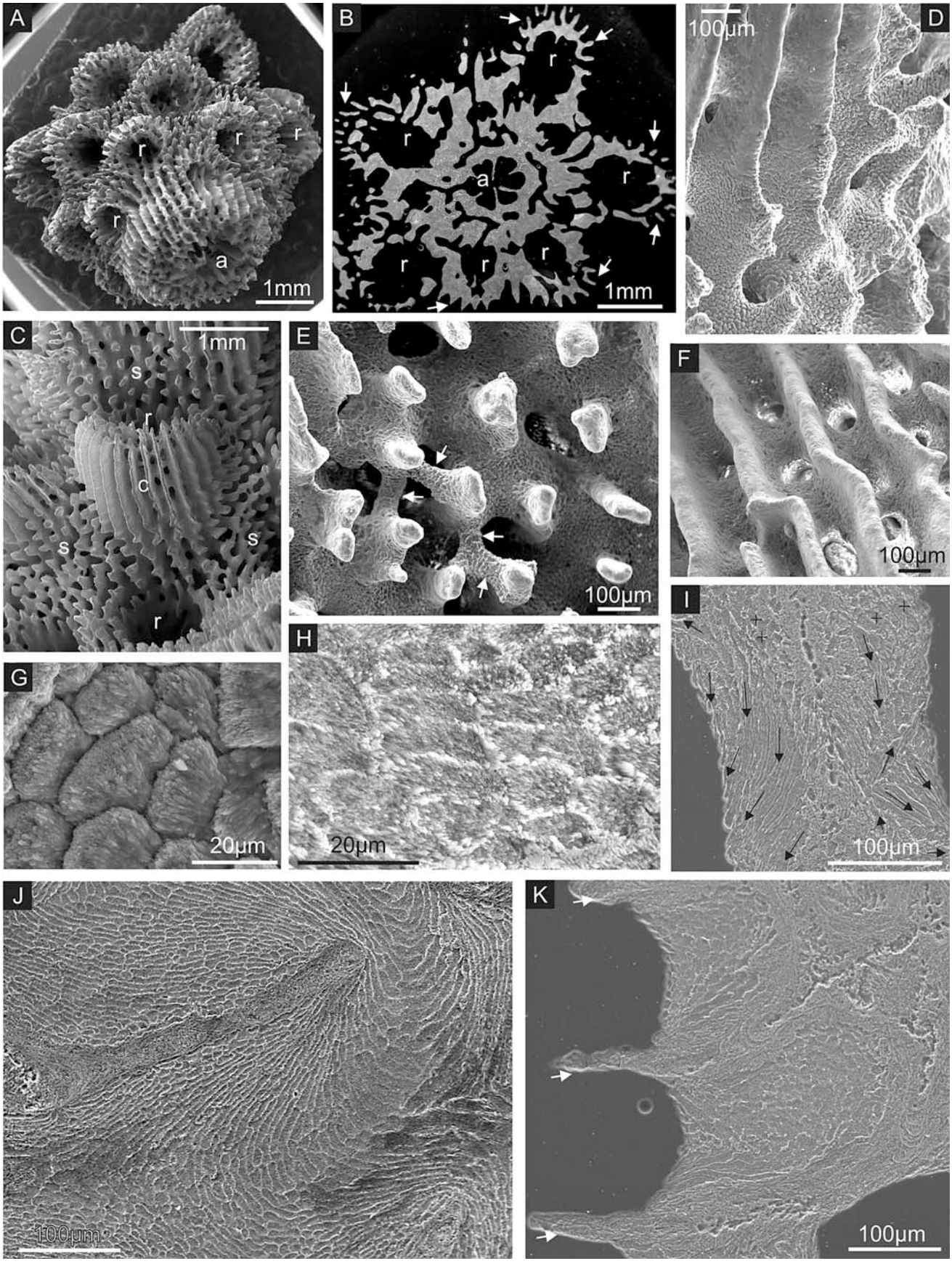
A
r
r
r
r
a
1mm
B
r
r
a
r
r
r
r
1mm
D
100µm
C
1mm
s
r
c
s
s
r
E
100µm
F
100µm
I
100µm
G
20µm
H
20µm
J
100µm
K
100µm

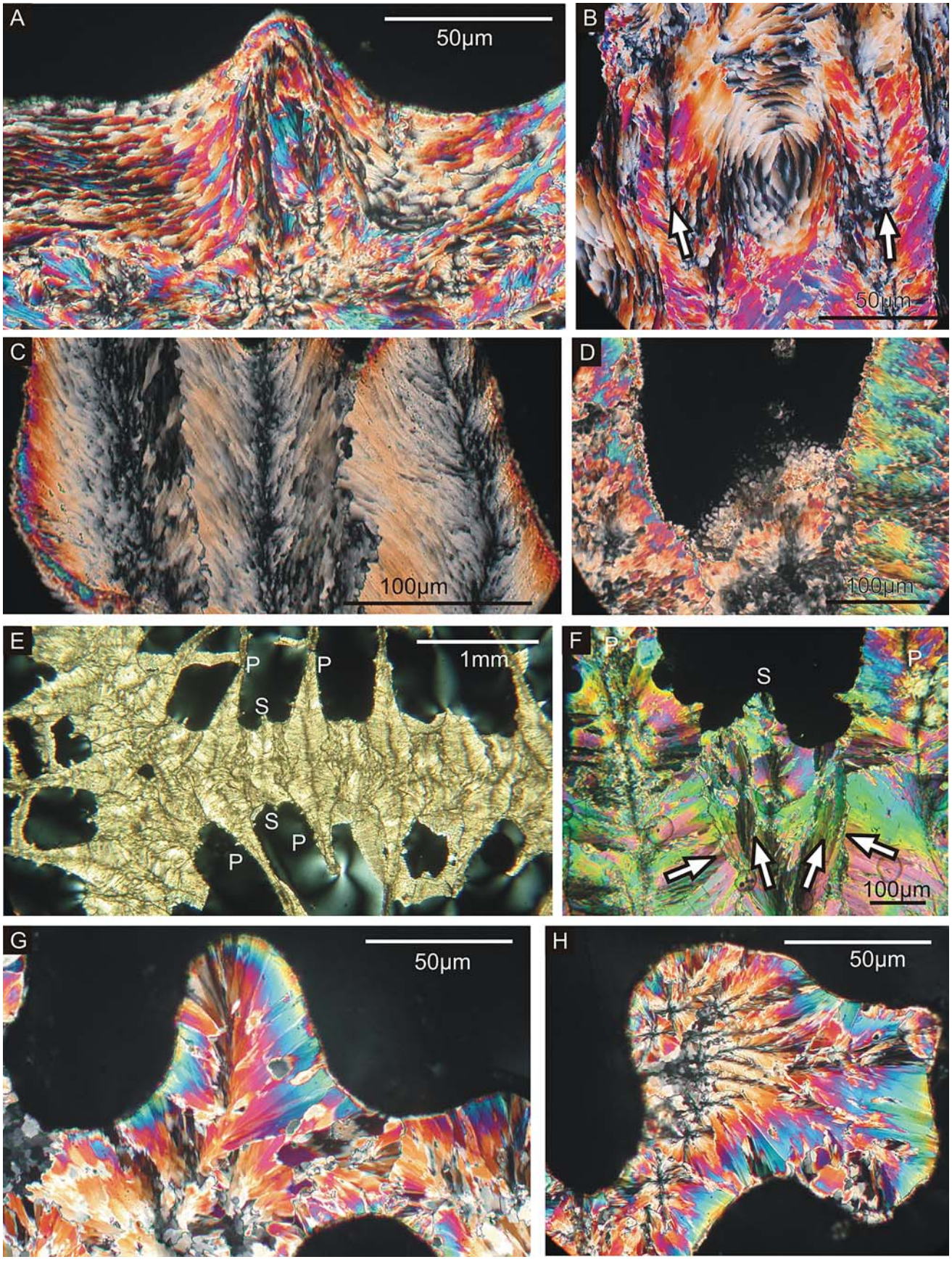
A
50μm
B
50μm
C
100μm
D
100μm
E
1mm
P
P
S
S
P
P
F
P
S
P
100μm
G
50μm
H
50μm

Walls are formed by an initial phase of skeletal growth involving fibrous trabeculae, followed by the filling of open inter-trabecular spaces by individual flattened, elongated bundles of fibers that occur at an oblique, low angle to the basal ectoderm resulting in a 'shingle-like' appearance (Sorauf 1972; Sorauf and Podoff 1977; Gautret et al. 2000; Nothdurft and Webb in press) (Figs. 5D–K, 6A–B). Outer surfaces of skeletal elements are covered by such shingles. Shingles appear to be better developed at bases of costae and spinules in the coenosteum, and the upper surfaces of these structures can be relatively smooth (Fig. 5F). Costae and spinules contain a layered/trabecular microstructure, and saddle-shaped depressions between them are partially filled by layers of shingles. Thus, trabeculae and space-filling shingles are intimately mixed spatially, but represent temporally disjunct skeletal deposition with shingles accreting at high angles to fibers in trabeculae along obviously disconformable surfaces (Fig. 5K). Skeletal thickening occurs in coenosteal areas where synapticulae are composed predominantly of shingles that grow from either side between two ridge-shaped costae, in some cases evenly, in other cases with one side dominant (Fig. 7). The initial growth direction of shingles in synapticulae is perpendicular to the growth direction of the costae. Once the two sides have made contact the structure continues to thicken, forming the dominant reticulate structure of the coenosteum. Layers of fibronormal microstructure are not prominent.

Individual shingles are 4–50 μm wide, 2–7 μm thick, and between 20 and 150 μm in length. However, because individual shingles have variable and curving growth direc-

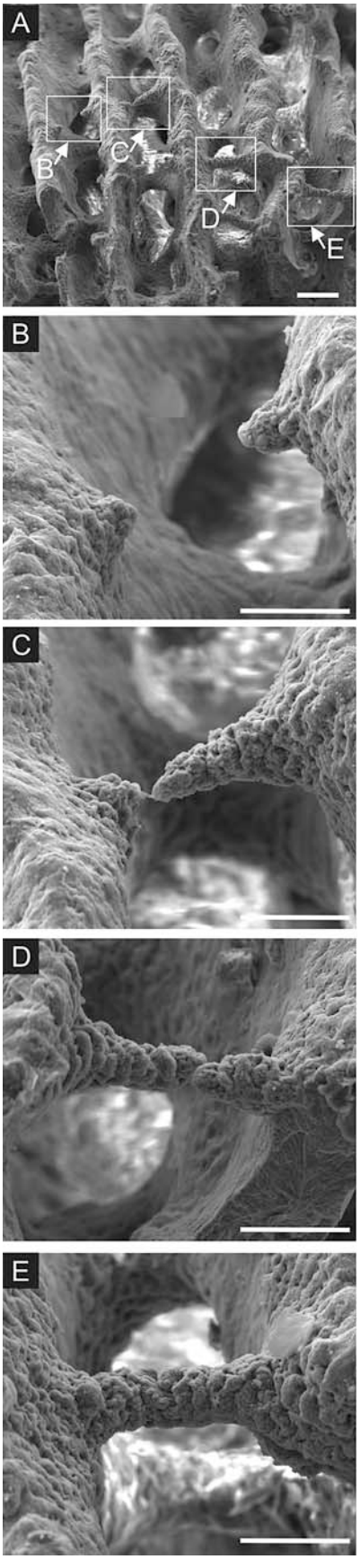

◀ **Fig. 6** Ultrathin sections of four coral genera showing differences in skeletal microstructure. **A** and **B** *Acropora hyacinthus*. **A** Transverse section showing shingle microstructure draped around trabecula microstructure of a costa/spinule similar to that seen in Fig. 5J, 5K. (sample 98-6-12C). **B** Longitudinal section through two costae (*white arrows*) illustrating shingle microstructure filling space between costae (sample 03-10-47). **C** and **D** *Pocillopora damicornis* (sample 03-10-83). **C** Longitudinal section through adjacent trabeculae. Note that fibers in trabeculae are already roughly grouped into bundles. **D** Longitudinal section though a calice illustrating the secondary filling of bundle microstructure at the base of the calice. **E** and **F** *Goniastrea favulus* (sample 04-9-30). **E** Transverse section illustrating primary (p) and secondary (s) septa with fibrous trabecular microstructure continuous between adjacent corallites. **F** Intergrowth of trabeculae in adjacent primary (p) and secondary (s) septa showing differences in growth direction of fibers (*white arrows*) and obvious discontinuity in age of adjacent skeleton. **G** and **H** *Porites lobata* showing continuous growth of trabecular fibers from the centers of skeletal elements to their smooth edges (sample 03-10-65). **H** Multiple adjacent trabeculae with finger-like projections on growth front

Fig. 7 Scanning electron photomicrographs of synapticulae development between costae in *Acropora hyacinthus* (sample 03-10-50). *Scale bar* is 20 μm except in **A** where it is 100 μm. **A** External lateral view of a radial corallite showing the location of synapticulae shown in **B**–**E**. **B**–**E** Progressive stages of growth of synapticula. **B** Initial stage of synapticula growth from either side of adjacent costae. **C** Initial connection by shingles across the two sides. **D** and **E** Progressive thickening of synapticulae as they are coated by shingles oriented at right angles to corallum extension. Continued thickening of synapticulae will fill the space between the two costae, appearing like that shown in Figs. 5F and 6B ▶

tions that are commonly oblique to the plane of ultrathin or polished sections, it is difficult to observe shingles in their entirety from their point of nucleation to their termination. Hence, the greatest length attained by shingles is unknown. Fibers within shingles are roughly parallel to the surface of underlying shingles and radiate laterally at angles between 6 and 45° with low angles dominating (Fig. 5G). Where fibers are roughly parallel (i.e., low angle of divergence), they appear to be in optical continuity and may not be distinguishable in ultrathin sections that intersect them at high angles (Fig. 6A–B). Hence, in many cases shingles appear to be single crystals in cross-polarized light despite their clearly fibrous internal structure. Preferential etching on surfaces of shingles enhances thin growth lines similar to those in fibers in trabecular regions (e.g., Cuif and Sorauf 2001).

Most shingle growth is directed distally within each corallite, not directly away from individual surfaces, and growth directions are non-parallel on surfaces with complicated relief. Some shingles appear to originate from the distal edges of trabeculae, where they are continuous with fiber bundles within the trabeculae, but most occur against trabeculae with distinct discontinuity (Fig. 5I). It is commonly unclear exactly where shingles nucleated, but numerous layers of shingles fill relatively large spaces between trabeculae, in some cases, more than 25 layers deep (Fig. 5J–K). In ultrathin sections, *Acropora* shingles are similar in size and appearance to lamellae-microlamellae in Paleozoic corals, commonly having roughly crescent-shaped transverse cross sections (Nothdurft and Webb in press).

In polished and etched sections, the outermost edges of shingles are more resistant to acid etching than the inner parts emphasizing the shingle structure in SEM images (Fig. 5H). Sorauf (1972) suggested that shingles were surrounded by organic material, and Cuif et al. (1997) suggested that the etching pattern results from an intracrystalline organic coating in the fringes of the structures that was protected from the oxidizing agent (NaOCl) during initial removal organic matter. Gautret et al. (2000) confirmed that interpretation by demonstrating the correlation of acridine orange staining, which reflects the position of calcium-binding organic matter, with the regions that stand in relief. Hence, individual shingles appear to be contained within organic envelopes.

Dissepiments are thin and weak and rarely exceed 12 μm in thickness. The upper surface is generally covered with shingles oriented obliquely towards a central ridge, whereas the under surface has a rough fibrous, 'furry' appearance with fibers orientated towards a central junction. The spacing between dissepiments is difficult to measure because sections of continuous corallites are rare. However, they appear to be irregularly spaced and can be as closely spaced as 330 μm.

Pocillopora damicornis microstructure

Coralla of *Pocillopora damicornis* are branching with compact robust branches tending to be slightly flattened or clavate. Distinction between verrucae and branches is difficult. Corallites are plocoid and range in diameter from 1–1.5 mm and can be slightly elongate in the dominant lateral growth direction of the branch. Calice depth ranges between 0.8 and 1.8 mm (Fig. 8A–B). Blunt, cone-shaped spines up to 150 μm long cover the coenosteum. Spines located on the outer margin of the corallite line up with septa (Fig. 8A–C). The width of the septal wall is variable within a single branch, ranging from 80 to 700 μm. The walls are generally thicker on lateral corallites of the branch. Corallites have septothecal walls, poorly developed septa, and no columellae. Some septa have well-developed dentition or spines (Fig. 8D). Spines extend perpendicular to the wall towards the centre of the corallite in line with, and along, septa and are generally larger at the base of the corallite. Larger spines are cone-shaped and up to 120 μm long and 80 μm wide at the base with blunt rounded tips. Less well developed spines range down to mere bumps. The degree of spine development is variable within coralla with some corallites and inter-septal spaces having well-developed spines, and others having none.

Fig. 8 Scanning electron and thin-section photomicrographs of ▶ *Pocillopora damicornis*. **A** Exterior view of corallum showing size, shape, and structure of corallites. The coenosteum is covered by cone-shaped spines of varying sizes. Also note the variable thicknesses of the theca where the wall labelled (a) is approximately 650 to 700 μm across while the wall marked (b) is less than 100 μm thick. Septal spines occur in vertical rows on calice walls (sample 03-10-71). **B** Longitudinal section through a branch showing distally convex dissepiments (d), septal spines and coenostial spines at the top of the calices (sample 03-10-80). The box indicates the location of **C**. **C** Higher magnification view of coenostial spines shown in **B**. The spines are prominent, conical in shape and covered with terminations of bundles. **D** Longitudinal view of internal calice wall showing septal spines forming a row. The spines and the surrounding area are covered by bundle terminations except where the coral polyp has left an attachment scar (as) (sample 03-10-80). **E** High magnification view of the bundle terminations that cover most surfaces of the *Pocillopora damicornis* skeleton. They are more irregular in size, but more equant in shape, than the shingles in *Acropora hyacinthus* (Fig. 5G), and are less ordered in arrangement (sample 03-10-80). **F** Polished and etched longitudinal section through the theca. Section shows three coenostial spines that have EMZ in a layered appearance that is distinct from thickening by fiber extension of individual trabeculae by bundles (sample 03-10-90). **G** Polished and etched transverse section through a branch showing spines (*black arrows*) that have layered trabeculae. The spaces between spines are filled by bundle microstructure. As in *Acropora*, aragonite fibers on the outer edge of bundles etch in higher relief than fibers in the inner parts (sample 03-10-92). **H** Thin section photomicrograph in crossed polarized light of primary trabeculae of the theca (*large black arrow*) and secondary trabeculae (*small black arrows*) growing at 90° to the theca. Secondary trabeculae fill in space within the calice and are topped by spines (sample 03-10-92). **I** Slightly oblique longitudinal section of an inter-septal space and the underside of a dissepiment (d). The dissepiment displays centripetal growth culminating in a central junction that takes the form of a groove. The septal wall and spines under the dissepiment are covered by bundles. The area above the dissepiment, indicated by the dashed line, is completely filled by thickening deposits (sample 03-10-92). **J** Thin-section photomicrograph in plane polarized light of a dissepiment showing convex shape and central 'keystone' (sensu Jell 1974). Note that the septa are considerably thicker above the dissepiment than below it due to continued fiber extension subsequent to emplacement of the dissepiment (sample 03-10-92)

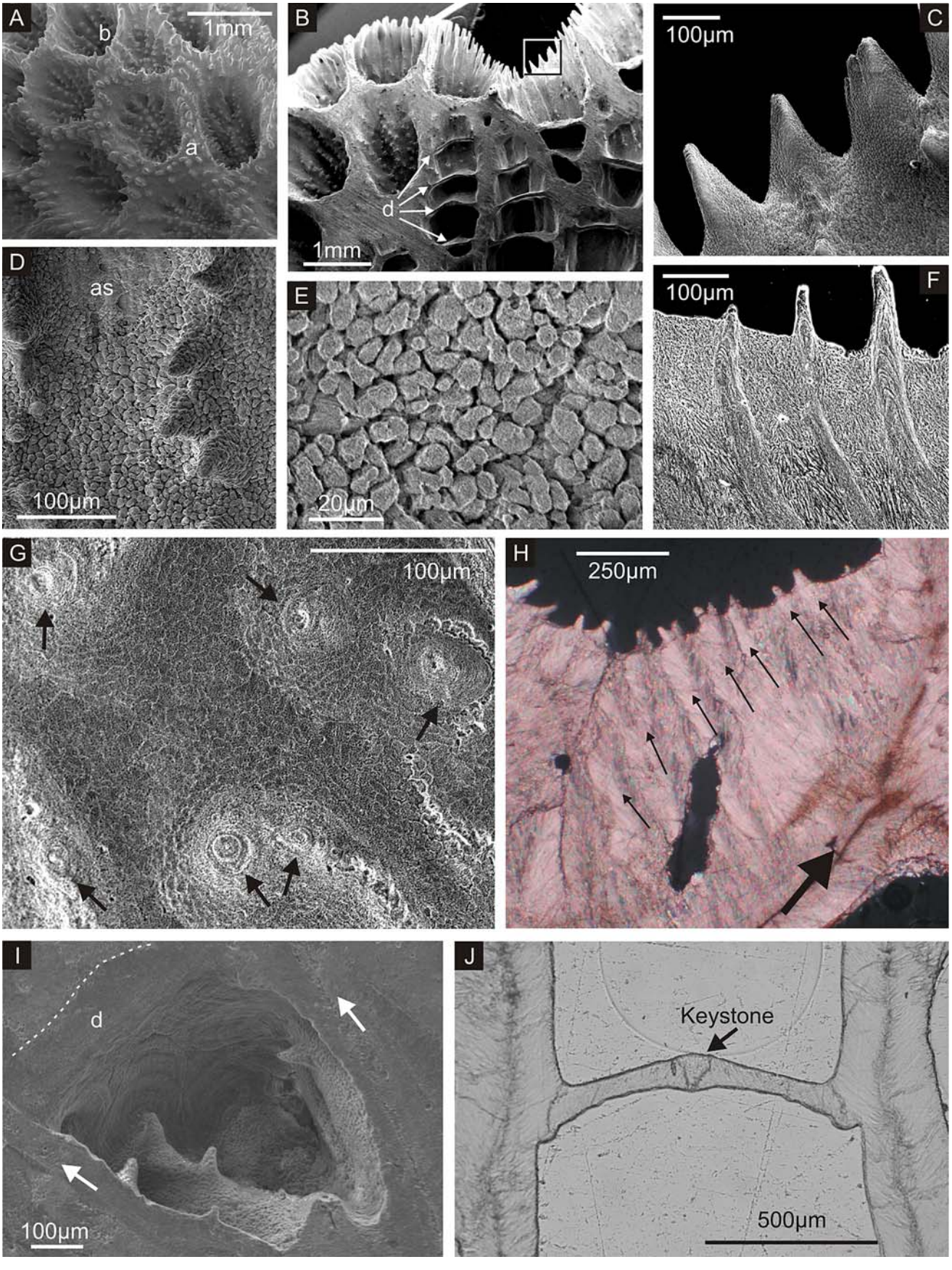
A
b
1mm
a
B
d
1mm
C
100µm
D
as
100µm
E
20µm
F
100µm
G
100µm
H
250µm
I
d
100µm
J
Keystone
500µm

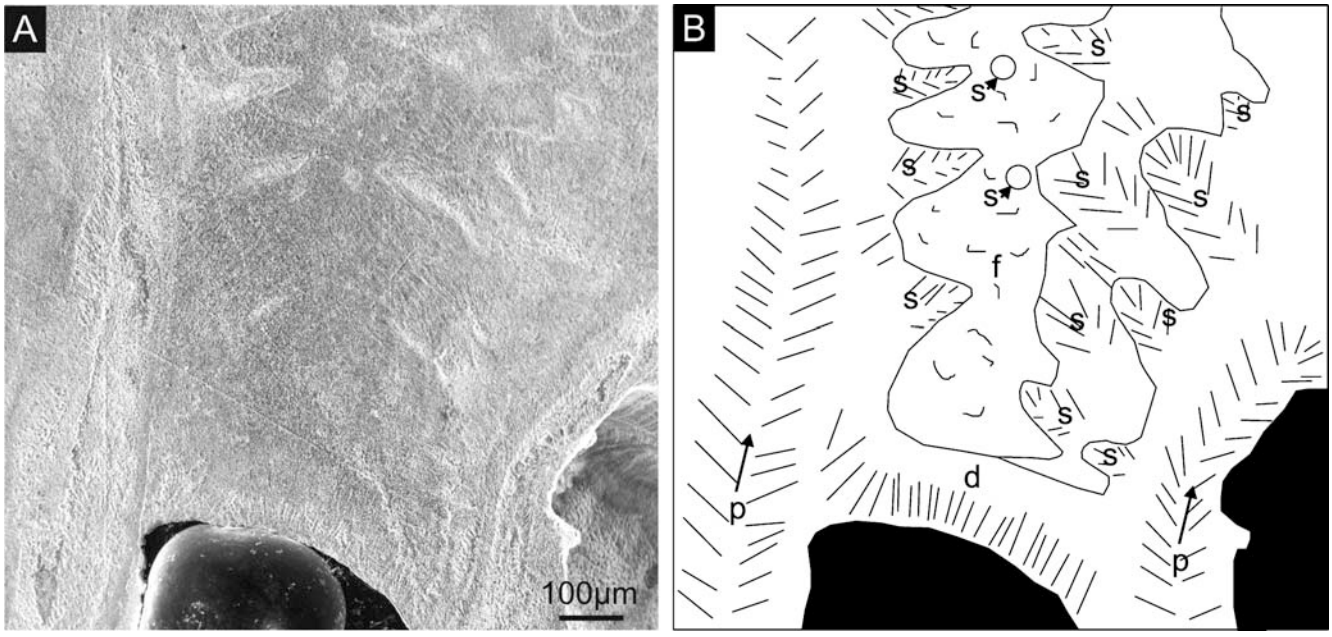

Fig. 9 Microstructure of *Pocillopora damicornis*. **A** Scanning electron photomicrograph of polished and etched longitudinal section (sample 03-10-72). **B** Schematic diagram of **A** showing the primary trabeculae (p) occurring as septa and secondary trabeculae (s) branching off from the primary trabecular into the inter-septal space above the dissepiment. The remaining intra-calical space is filled by thickening deposits composed of bundles (f)

Trabeculae have radiating fibrous microstructure, but fibers within trabeculae are commonly grouped into bundles (Fig. 6C). Trabeculae may be simple, if there is only a single "axis of calcification", or compound, if secondary axes are developed. Secondary trabeculae diverge from primary trabeculae at acute to nearly 90° angles and end as spines that project into the calice (Figs. 8H, 9). Intergrowth of adjacent spines results in sections of dense skeleton with little or no inter-septal space remaining. Thickening is best-developed on flanks of branches.

External surfaces of calices and coenosteum, including spines, are generally covered by irregular, dome-shaped fasciculi (Wise 1970; Vandermeulen and Watabe 1973) (tufts sensu Jell 1974, in the genus *Fungia*) (Fig. 8C–E). The fasciculi represent the ends of bundles of skeletal fibers, which may or may not be slightly radiating, and are somewhat more elongate at the base of the calice than at the tip. In the transverse section, individual bundles range in shape from circular, to oval, to crescent-shaped, or irregular-shaped, and aggregates of as many as three or four tufts occur fused together (Fig. 8E). Bundle diameters range from 5 to 30 µm and in some cases they can be traced directly into trabeculae. While similar in appearance and size to the shingles in *Acropora*, bundles in *Pocillopora* have a far less ordered arrangement and tend to be more equidimensional, but irregular in shape. The outermost margins of bundles stand in relief in polished and etched sections, but less so than around the shingles in *Acropora*. Studies have not been carried out yet to determine if the poorly etched zones result from increased organic matter, as in *Acropora*. However, this is probably the case.

Polished and etched longitudinal sections cut perpendicular through the theca of *P. damicornis* show simple trabecular microstructure. Fibers diverge from stacked 'centers of calcification' at between 60° and 90° (Fig. 8E–H). Thin walls are only one trabecula thick, whereas thicker walls may have several trabeculae joined laterally (Fig. 6C–D). The theca generally has a growth front composed of coenostial spines that reflect the position of trabeculae (Fig. 8C, F). In etched sections (Fig. 8F) the spines appear to be disjunct from secondary thickening, and they stand in

Fig. 10 Scanning electron photomicrographs of *Goniastrea favulus*. **A** Longitudinal section through a corallite illustrating skeletal elements: theca (t), dissepiment (d), columella (c), septa (s), paliformal lobes (p) (sample 04-9-30). **B** View within calice illustrating relationship between paliformal lobes (p) and septa. Septa have dentition with rows of verpreculae (*dashed lines*) along the side of the septa in a line towards the denticles (sample 04-9-30). **C** View along the thecal wall showing septa and their dentition fanning from one corallite to the adjacent corallite (sample 98-6-12B). **D** High magnification view of dentition at the edge of septa showing pointed tips on the margin of each septum that fan out to form fist-like shapes perpendicular to the septal plane (sample 98-6-12B). **E** Transverse polished and etched section of theca and corallites showing cross sections of those features shown in **A** (sample 04-9-30). **F** Higher magnification view of a transverse section of theca and septa. The EMZ are fairly continuous (*dashed white line*) both along the theca and within individual septa. *Solid black lines* show individual growth lines in fibrous microstructure (sample 04-9-30). **G** Polished and etched longitudinal section across a thecal wall. *Black lines* trace growth lines illustrating the layered nature of thickening deposits. *Dashed sections* indicate uncertainty in the exact location of the growth line (sample 04-9-30). **H** and **I** Polished and etched sections of the EMZ in longitudinal (**H**) and transverse (**I**) sections. Note the continuity of preferentially etched organic matter-rich layers in the centers of trabeculae with growth lines in the fibrous thickening layers (sample 04-9-30) ▶

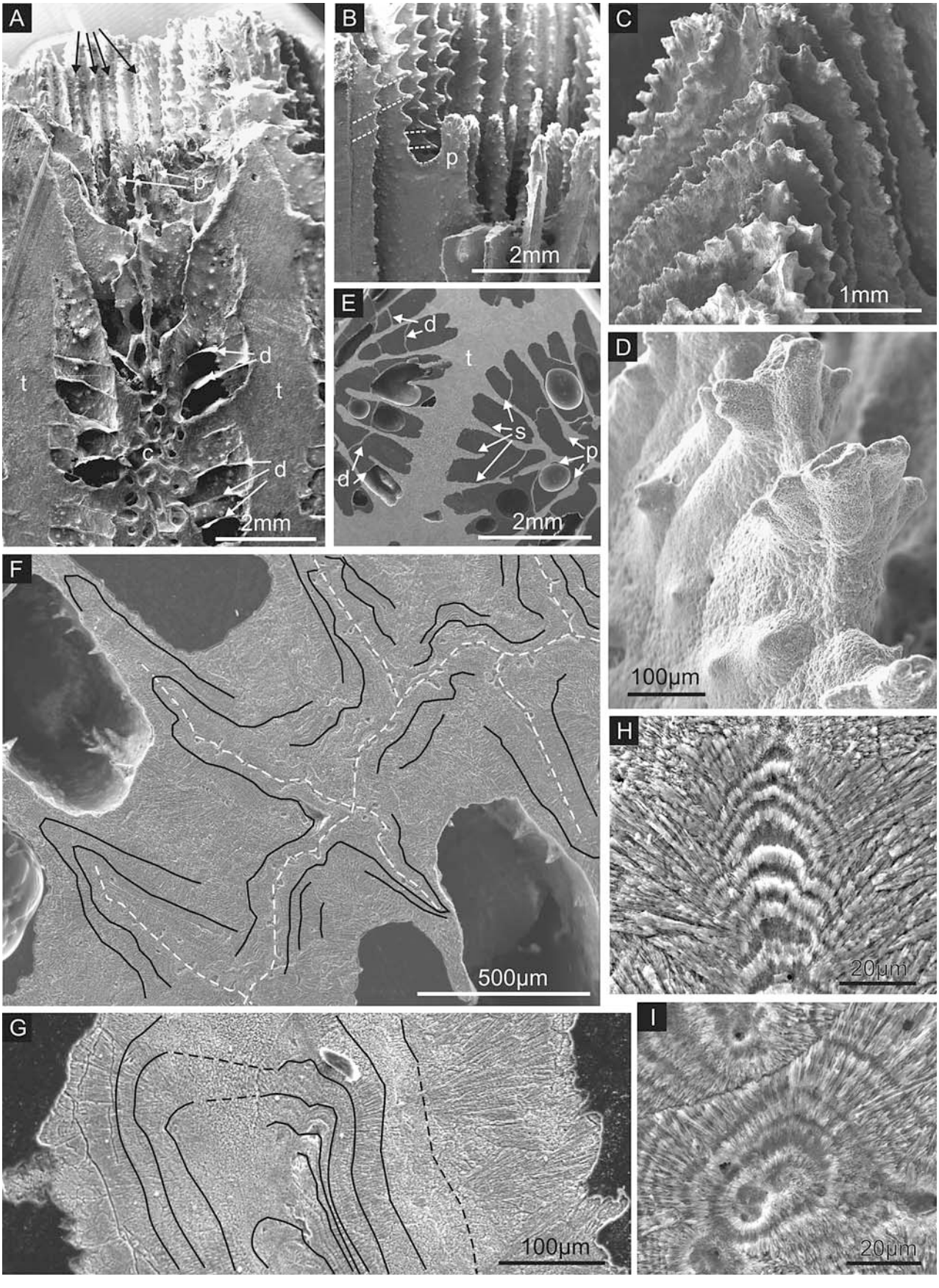
A
p
d
t
t
c
d
2mm
B
p
2mm
C
1mm
E
d
t
s
p
d
2mm
D
100µm
F
500µm
H
20µm
G
100µm
I
20µm

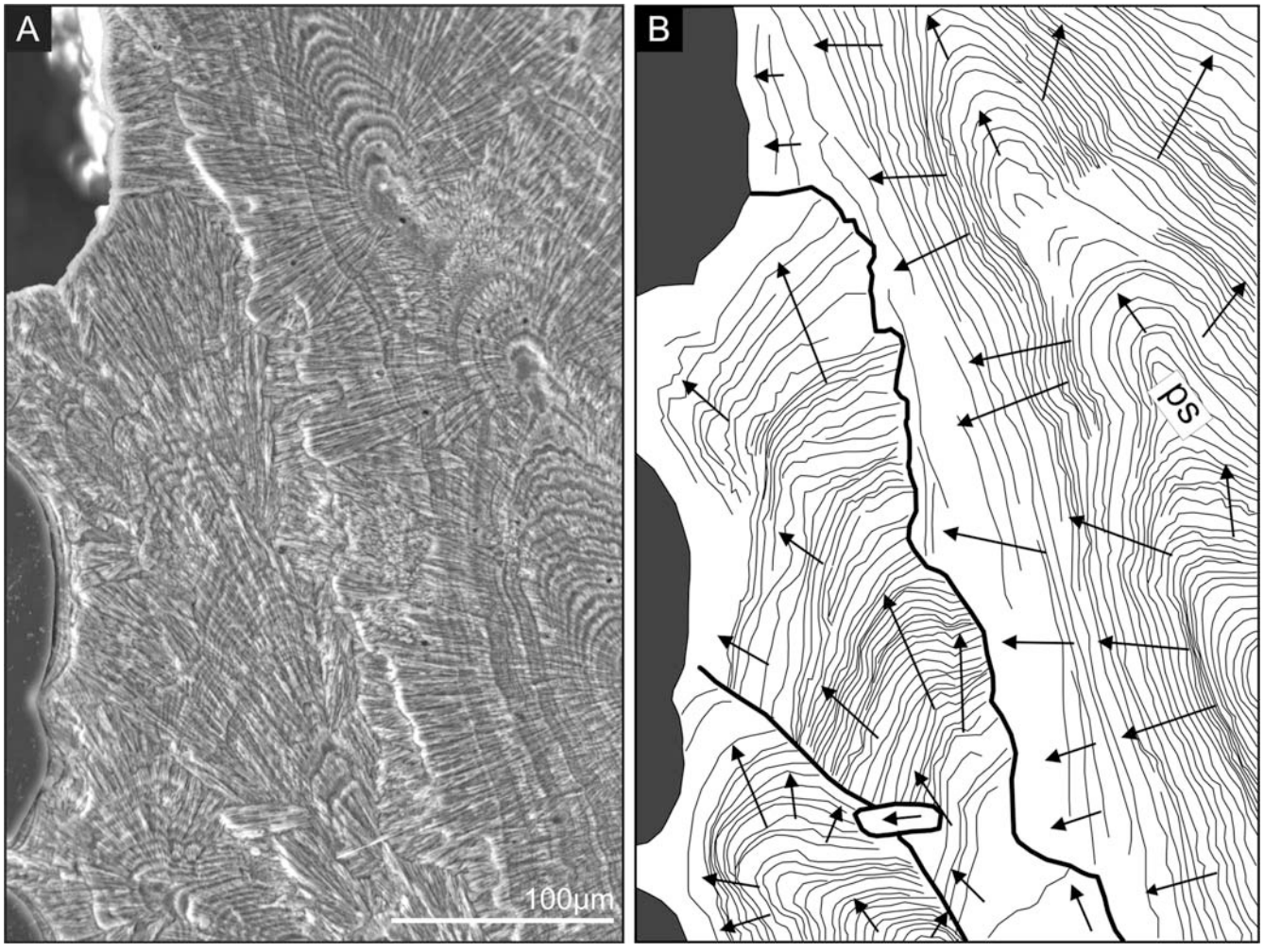

Fig. 11 Microstructure of *Goniastrea favulus* showing obvious discontinuity between fibers of the septa and fibers in the thickening layer that forms the theca. **A** Polished and etched transverse section of theca (sample 04-9-30). **B** Schematic diagram traced from **A** to show growth lines within primary septa (ps) and adjacent fibers. Growth direction of fibers is shown by the *arrows*

relief at the surface of the corallum, but in petrographic and ultrathin sections, the thickening appears to result from extension of fibers in trabeculae without obvious disjunction (Figs. 6C, 8H).

Pocillopora damicornis has endothecal dissepiments that are generally equi-dimensional or slightly elongate in the direction of primary growth of the branch (Fig. 8I–J). They are convex distally with a relatively smooth underside and a variable upper surface. The undersides display centripetal growth from each side of the corallite wall bounded by lateral junctions (sensu Sorauf 1970: Fig. 2) and culminating at a central junction that is typically an elongated central groove or, rarely, a single point of depression. The upper surfaces of dissepiments are variable depending on

Fig. 12 Scanning electron photomicrographs of *Porites lobata*. **A** Distal view of ceroid corallites. The *white box* is the area shown in ▶ **B** (sample 03-10-79). **B** Single corallite showing the internal structure. The *white box* is the area shown in **D**. **C** (sample 03-10-65) and **D** (sample 03-10-79) Vertical skeletal elements of septa (s), pali (p), and columella (c), all with finger-like extensions at the tips on the surface. **E** Spines form the beginnings of synapticulae between vertical elements of the skeleton and are an extension of fanning fingers such as those shown in **C** and **D** (sample 03-10-79). **F** Polished and etched longitudinal section showing the columella (c) in the middle of the calice. The base of the calice is marked by the last-formed dissepiment (d) (sample 03-10-76). **G** Polished and etched longitudinal section of a septum. *Solid black lines* represent EMZ, and their distribution shows that they are not continuous throughout the septum. The areas above dissepiments (d) have thickening that clearly post-dates the formation of the adjacent parts of the septum. *Dashed black lines* indicate the edge of the septum before the formation of the dissepiment. *White arrows* indicate places where the edges of the septum and dissepiments have been covered by non-skeletal aragonite in the form of syntaxial early marine cement. Despite cements commonly being in optical continuity with skeletal aragonite they can be distinguished by their coarser fibrous texture (sample 03-10-65). **H** Broken and etched transverse section through a septum showing the EMZ and radiating fibers in the trabecula. Note the microboring (sample 98-6-12G). **I** Broken and etched transverse section through vertical elements of skeleton showing multiple EMZs, each with radiating trabeculae abutting each other but forming a smooth outer surface where fibers terminate in unison as fibronormal microstructure (sample 98-6-12G). **J** Polished and etched longitudinal section of the hand-shaped tip of a septum with finger-like extensions and multiple adjacent trabecular. The *white arrow* indicates direction of corallite extension (sample 03-10-65)

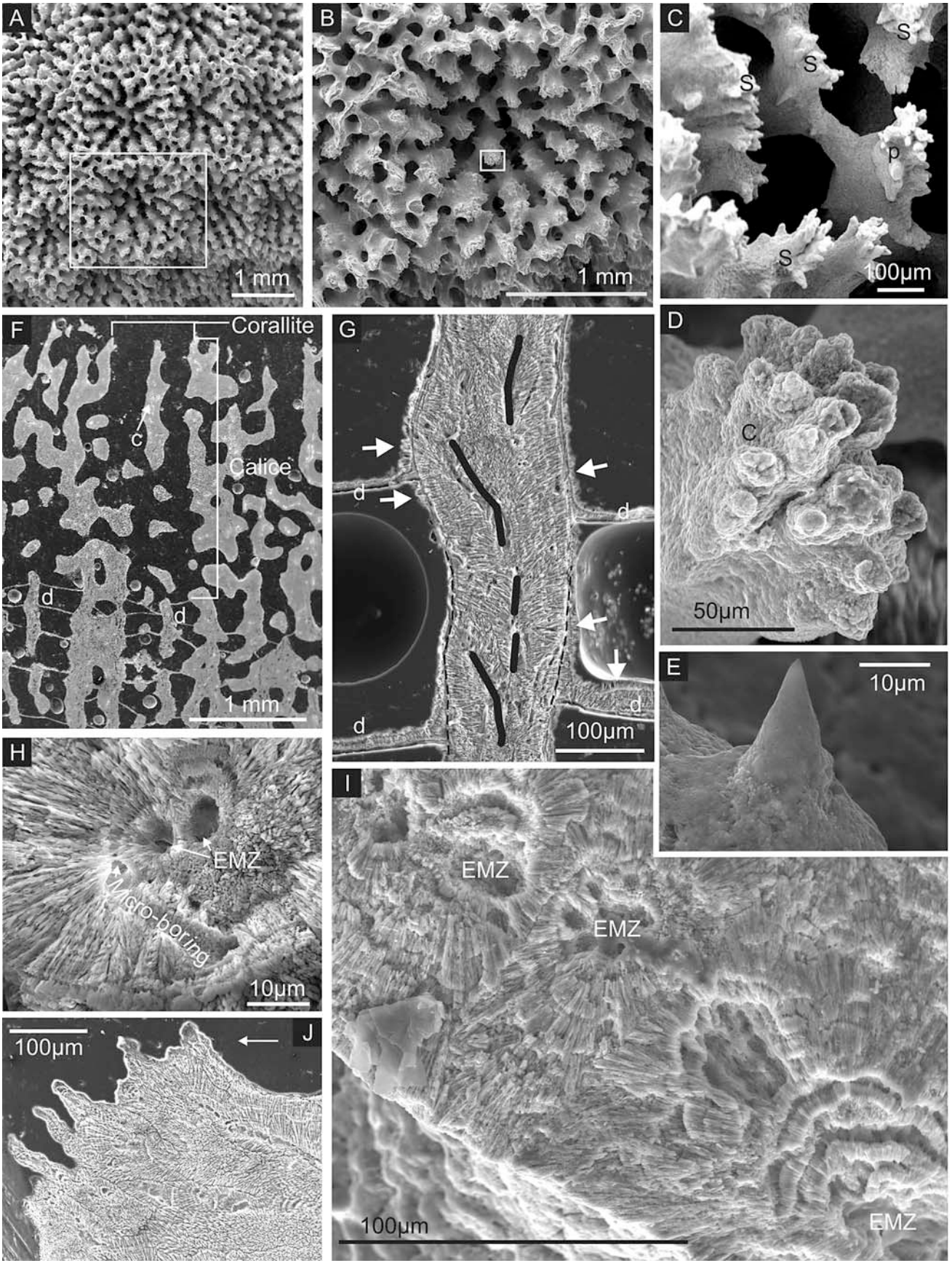
A
1 mm
B
1 mm
C
S
S
S
p
S
100µm
D
C
50µm
E
10µm
F
Corallite
c
Calice
d
d
1 mm
G
d
d
d
d
100µm
H
EMZ
Micro-boring
10µm
I
EMZ
EMZ
100µm
EMZ
J
100µm

the amount of subsequent thickening. Non-thickened dissepiments have a smooth upper surface, but thickened dissepiments have nodular surfaces with structures that can be described as bundles. The apparent bundles are directed obliquely towards the center of the calice and distally. Bundles do not mimic the arrangement of centripetal fibers seen on the under surface. Thickening of septa commonly occurs immediately above dissepiments so that septal flanks distinctly step inward immediately above dissepiments at the base of the calice (Fig. 8J). The average vertical spacing between dissepiments is 585 μm ($\sigma = 178$), ranging between 200 and 1,000 μm.

Goniastrea favulus microstructure

Goniastrea favulus colonies are massive, and all colonies sampled in this study have small (< 10 cm), dome- or ovoid-shaped coralla. Corallites are mostly submeandroid to cerioid (e.g., see Veron 1986). Corallites range in diameter from 3 mm in smaller cerioid corallites to submeandroid corallite groups up to 20 mm long. Most corallites are between 5 and 10 mm in diameter. Calice depth is between 5.5 and 7.5 mm. The thecal wall is generally 600–800 μm thick, thinning towards the tip of the calice (Fig. 10A–I).

Goniastrea favulus has at least two cycles of septa and probably a third in some corallites (Fig. 10E–F). Septal dentition is present on all septa, but more pronounced on primary septa (Fig. 10B–D). Dentition comprises pointed tips on the margin of each septum that fan out to form fist-like shapes perpendicular to the septal plane. In lower parts of the calice, denticles become increasingly developed towards the axial margin and eventually twine together to form a columella. In cross section, denticles represent the primary growth points of trabeculae. Lines of verpreculae (sensu Jell 1974) are aligned with the denticles at the margin along the lateral face of most septa (Fig. 10B). These verpreculae represent secondary trabeculae that branch off perpendicular to the primary septum.

Septa are continuous over the thecal wall between adjoining corallites (Figs. 5E, 10E–F). The upper portions of the axial edge of the septal plane of most septa (upper 2–4 mm of the calice) parallel the theca. Primary septa in the lower parts of the calice extend farther towards the center of the calice to form a weak lobe. The direction of growth of septa and denticles in this area changes from perpendicular to the theca to an upward oblique direction, and from this point, denticles extend farther and intertwine to form a columella.

Septal thickness narrows from the edge of the theca towards the center of the corallite. Where primary and secondary septa join the theca, widths are consistent at ~240–260 μm. Septa narrow gradually for the first 500–700 μm away from the theca to a width of 80–100 μm near the center of the calice. Secondary septa terminate at 500–700 μm from the theca; primary septa continue at a similar thickness farther into the calice.

At the thecal and septal margin, there is obvious discontinuity between fibers of the primary structures and fibers in thickening deposits. Trabecular fibers in the thickening deposits are oriented parallel or at a low angle to the theca and septa and are disjunct from earlier trabecular fiber growth that is perpendicular to the surface of the theca or septum as is obvious in the configuration of growth lines in the fibers (Figs. 6F, 11). Trabeculae tend to be adjacent and parallel in the septotheca, and bundle-like structures that provide thickening between trabeculae in *Acropora* and *Pocillopora* appear to be lacking. Where thickening occurs, it appears to represent a continuation of trabecular fibers.

Dissepiments are endothecal and are strongly convex distally with centripetal growth lines on the underside. The underside is marked by a central groove, which is capped by a central keystone (as illustrated in Fig. 5 by Sorauf 1972; Jell 1974: Fig. 10). Sub-vertical thecal dissepiments are also present. The average vertical spacing between dissepiments is 522 μm ($\sigma = 113$), with a range of 180–720 μm.

Porites lobata microstructure

Porites lobata is a massive coral with dome- or hemispherical-shaped colonies. Specimens collected for this study were all parts of small (< 5 cm) coralla. Corallites are ceroid and 1–1.5 mm in diameter, and the calice depth is between 1.8 and 2.5 mm. Columellae, pali, and septa are present, and denticles form the outer part of the corallite and theca (Fig. 12A–I).

Columellae, pali. and denticles represent vertical elements of skeletal growth, all of which are similar in appearance being composed of finger-like extensions of fibers (15–30 μm long) with tips pointing distally and into the calice. Short and rounded individual 'fingers' splay out in places to form vaguely fist- or hand-like shapes (Fig. 12B–D). The majority of external surfaces of septa and walls are relatively smooth. However, spines extend out from margins of septa and denticles. Spines, which are larger than 'fingers', are sharp-tipped cone-like structures that are generally 25–30 μm long (Fig. 12E).

Denticles and pali join to form septa, whereas free-standing septa have a fascicular edge or growth front. Adjacent denticles also can be connected by radial skeletal growth in several layers along the margin of the corallite. All skeletal elements are composed of single radiating trabeculae (Fig. 12F–H). Most trabeculae are orientated distally, but those forming denticles occur at acute angles. Fibers in individual trabeculae radiate outwards terminat-

Fig. 13 Scanning electron photomicrographs comparing microstructure of four coral genera in polished and etched sections. *Scale bar* is 100 μm for all images. **A** and **B** *Acropora hyacinthus* with trabecular costae or spinules (p) as the primary skeletal framework and spaces between then subsequently filled by shingle microstructure (s) (samples 03-10-44 and WH-10). **C** and **D** *Pocillopora damicornis* with trabecular spines (p) as the primary skeletal growth element followed by growth of fiber bundles as extensions of trabeculae (s) (samples 03-10-90 and 03-10-47). **E** *Goniastrea favulus* with primarily layered trabecular growth in this longitudinal section through a theca (sample 04-9-30). **F** *Porites lobata* with relatively simple trabecular growth showing distinct growth lines in this longitudinal section through a columella (sample 03-10-65)

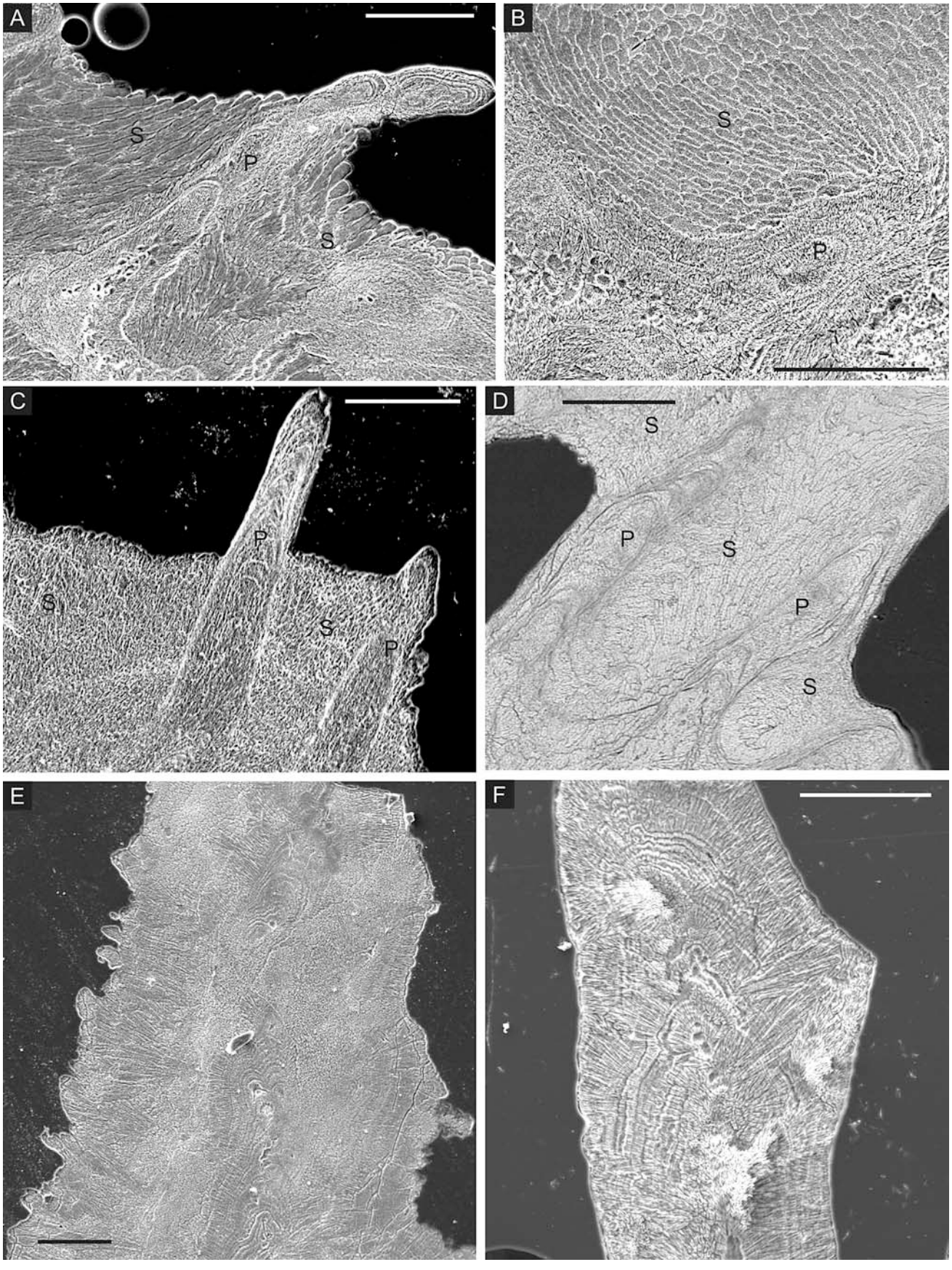
A
S
P
S
B
S
P
C
P
S
S
P
D
S
P
S
P
S
E
F

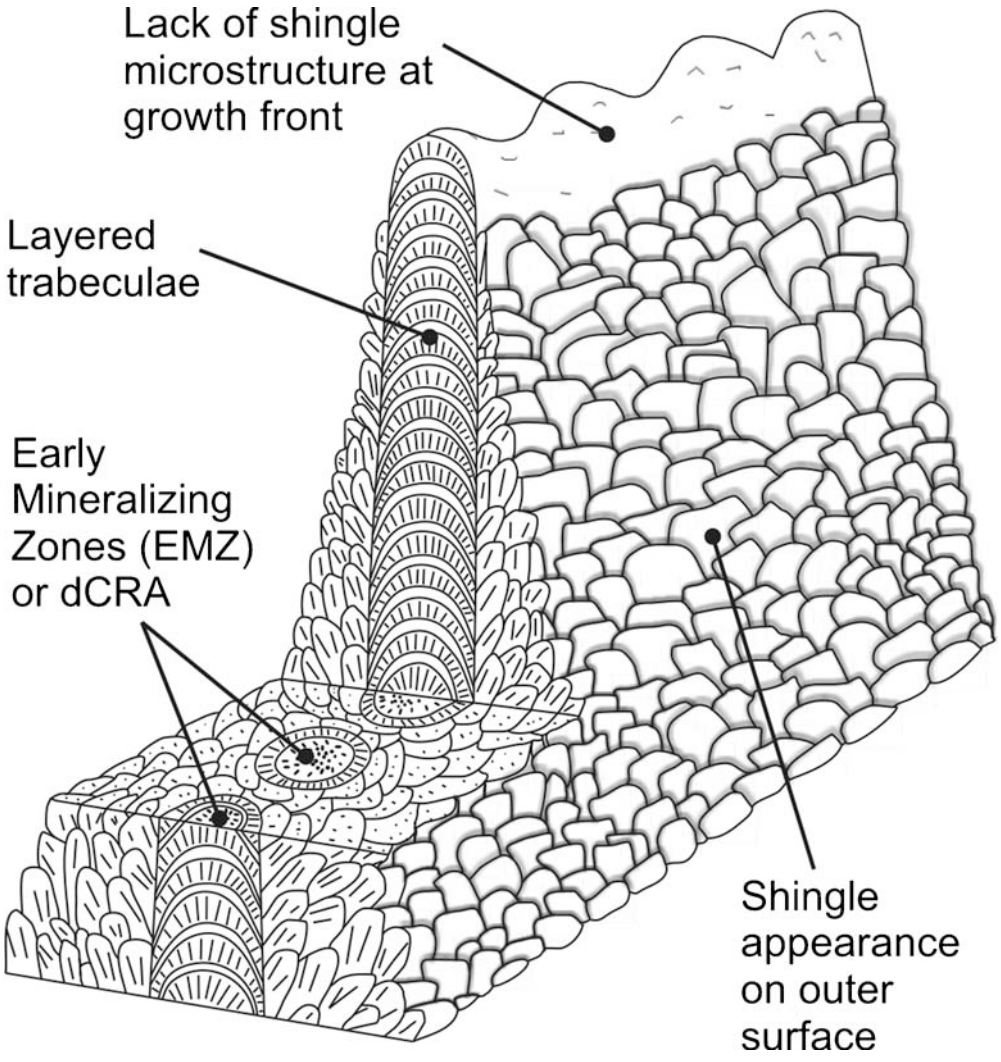

Fig. 14 Schematic diagram of an idealized growth model proposed for *Acropora* where an initial stage of layered trabecular growth is followed by fiber growth organized into shingles that are almost parallel to the surface of the ectoderm in pockets

ing evenly at high angles to the ectoderm to form smooth skeletal surfaces characterized by fibronormal microstructure (Figs. 6G–H, 12I). Although 'fingers' occur on columellae, pali, and denticles, they represent the surface expression of fibers that are continuous into trabeculae (Fig. 12J). No distinct shingles or bundles occur as in *Acropora* and *Pocillopora*.

Dissepiments are generally horizontal (basal) to subhorizontal, and are much weaker or less robust and more irregular in shape and position than those in the previously described genera. The average vertical spacing between dissepiments is 269 μm ($\sigma = 113$), with a large range between 60 and 460 μm.

Discussion

Models of skeletogenesis

Current models for the growth of coral skeletons (Cuif et al. 1997; Stolarski 2003) highlight differences in the timing of growth of different skeletal elements. Advances from the traditional trabecular model to incorporate stepped growth and organic layering have greatly improved our understanding of coral microstructure. However, the present study highlights the complexity and spatial variability of skeletal growth in different coral genera at levels of organization far above the nanoscale of individual fibers (Fig. 13). One basic model of organo-matrix-controlled skeletogenesis may account for the formation of individual fibers in and out of EMZ, but a variety of different microstructural growth models are required to characterize the temporal relationships of particular associations of fibers within the skeleton. Such new models are required if coral skeletons are to be interpreted adequately to serve as repositories of temporally constrained geochemical data.

In *Acropora*, initial skeletal deposits are formed by distally directed trabeculae in septa, costae and spinules. Subsequent skeletal thickening consists of layers of discrete shingles that fill spaces and depressions and form synapticulae. Synapticulae join costae at regular intervals along the coenosteum and thicken and accumulate along flanks of the scaffold-like trabecular costae, while synapticulae connect spinules in varied orientations. Hence, trabecu-

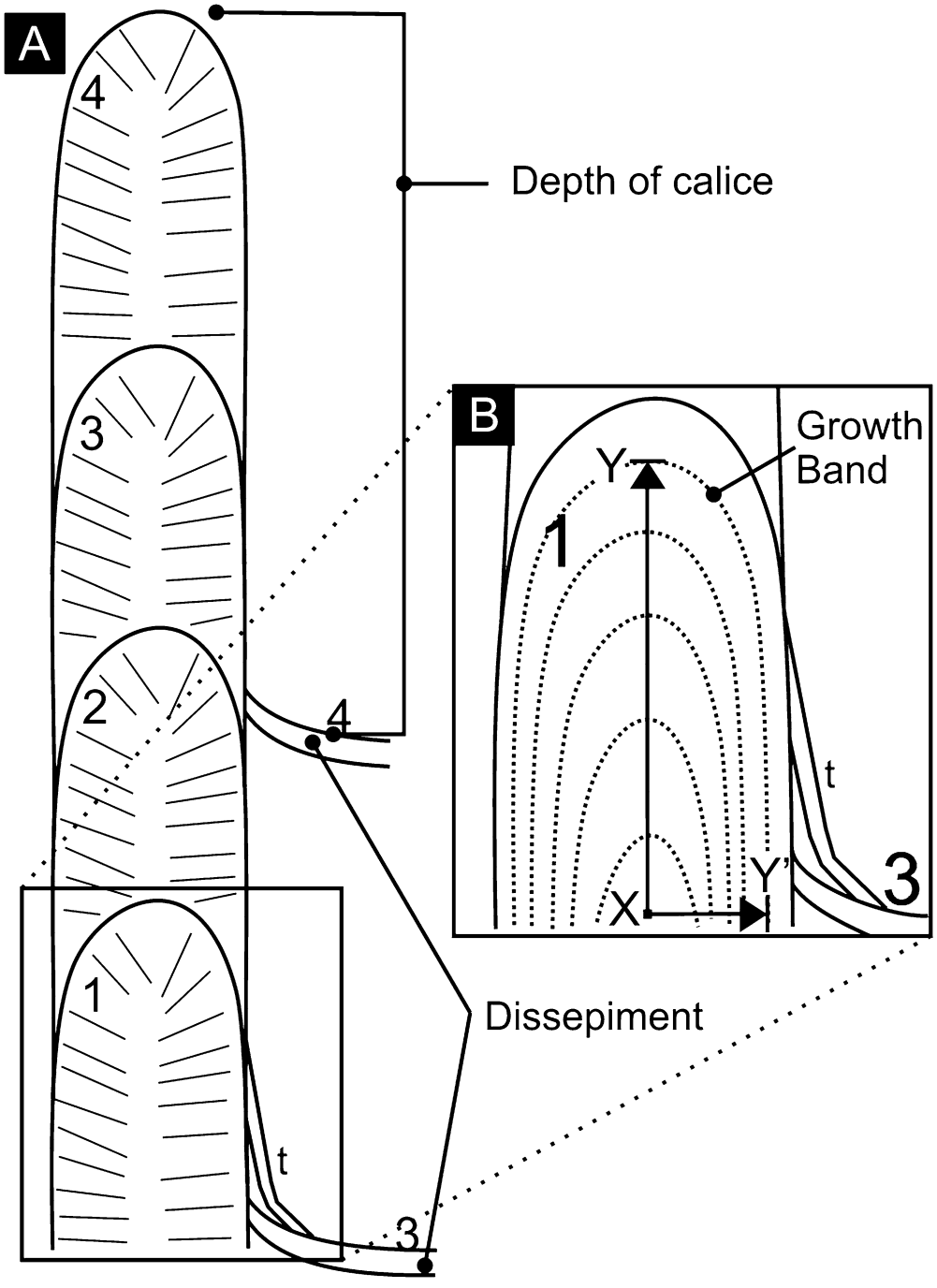

Fig. 15 Schematic diagram showing differences in timing associated with microarchitectural elements. **A** Large-scale microstructure through a septum showing broad temporal units numbered according to their time of deposition (1 oldest – 4 youngest). The emplacement of dissepiments and subsequent thickening of the septum above the dissepiment (t) creates a temporal disjunction between adjacent skeletal aragonite. In this example, parts of the septum deposited at time 1 are immediately adjacent to a dissepiment and subsequent thickening deposited representing time 3. **B** Enlarged view of lowest skeletal unit showing individual growth increments deposited during time 1. Note that growth lines show that vertical accretion at the center of the septum is more rapid than lateral accretion towards the flank of the septum. Therefore, the time series represented by line X–Y is equivalent to that represented by line X–Y'. Hence, even a slight excursion from the center of the septum towards the margin may lead to samples not representing true time series data

lar structures are intimately mixed spatially with zones of younger shingle microstructure. The conventional model for coral skeletal development involves extension of fibers from trabeculae or layered surfaces with elongation perpendicular to the basal ectoderm (Fig. 2). However, in *Acropora* the oblique fiber growth that forms the shingle microstructure occurs in pockets oriented at low angles to the overall ectoderm and direction of local extension. This type of skeletal accretion does not fit well within the range of previous microstructural models. Thus, a new model is

Table 1 Measurements of spacing between dissepiments and distance from the tip of the calice to the most recent dissepiment of three coral species*

Species	*Dissepiment spacing (mm)*			*Depth of calice (mm)*	
	Ave	Max	Min	Ave	SD
P. damicornis	0.59	1	0.2	1.2	0.5
G. favulus	0.52	0.72	0.18	6.2	0.6
P. lobata	0.27	0.46	0.06	2.2	0.3

*It was not possible to directly measure dissepiment data for *Acropora hyacinthus*

proposed here that involves a two-phased process with an initial phase of trabecular growth, followed by a secretory phase wherein spaces between trabeculae are filled, and surfaces are coated, by flattened bundles of fibers that grow at an oblique, low angle to the basal ectoderm, thus resulting in shingle microstructure (Fig. 14). Although we studied primarily *A. hyacinthus*, other *Acropora* species observed have similar microstructure, and the surface morphology that results from overlapping shingles is evident in photomicrographs of all other *Acropora* species illustrated by Wallace (1999). Importantly, because of the different orientation of skeletal fibers in trabeculae and shingles and their differing temporal relationships a linear transect of samples through a given skeletal structure need not yield time series data.

In *Pocillopora damicornis* dentition (spines) on the coenosteum and theca provide a growth front of layered trabeculae. Space between spines is filled subsequently by relatively equidimensional bundles making a microstructure similar to that of *Acropora* but with less apparent order. Thickening within the calice by emplacement of bundles between septa and septal spines proceeds to the point where bases of some calices are completely filled. Thus, a two-phase process similar to that in *Acropora* occurs in the genus, but the shapes and orientations of the bundles differ.

In *Goniastraea favulus,* initial growth consists of distally directed trabeculae forming dentition on the septo-thecal margin. Spines (dentition) on septa then extend laterally toward the center of the calice. Septal growth is characterized by strongly thickened, layered trabeculae, as in the traditional model of skeletogenesis. However, skeletal thickening between septa has different fiber orientations, providing clear evidence of multiple phases of temporally disjunct deposition (Fig. 11), but unlike in *Acropora* and *Pocillopora*, thickening deposits are not organized into bundles. Additionally, the intricate internal structure and relatively deep nature of the calice in *Goniastrea* contributes to a variable growth rate in different parts of the calice. The resulting microstructure is similar to that described by Cuif and Perrin (1999) in *Favia fragum*, also a member of the Family Faviidae.

Porites has the simplest microstructure of the genera studied. Trabecular fiber extension in *Porites lobata* occurs continuously over the surface of all skeletal elements and appears to be perpendicular to the surface of the basal ectoderm in all cases, thus forming sheets with fibronormal microstructure on the sides of vertical structures held up by trabeculae. Trabecular growth is layered and predominantly vertical, as in *Goniastrea,* but layering is less well developed. However, trabeculae in synapticulae are not invariably oriented distally and infilling and thickening of the skeleton between trabeculae occurs throughout the calice by extension of trabecular fibers. *Porites* has no fiber bundles, and the outer surface is relatively smooth. Thus, the *Porites* skeleton does not contain obvious temporally disjunct fiber associations within septa. However, septal thickening may occur continuously by extension of fibronormal layers at the base of the calice or on walls up until the time that a dissepiment is emplaced above the structure. At this time, the particular section of skeleton is sealed off from living coral tissue and can no longer grow. In some cases, irregularities in walls or septa are filled in by continued fiber extension in discrete patches wherein the growth lines that cut across fibers terminate laterally before passing into the EMZ of trabeculae. The exact time of em-

Fig. 16 Scanning electron photomicrograph of a polished etched ▶ section of *Porites lobata* (sample 03-10-65). **A** Photomosaic spanning the length of one continuous vertical section of skeleton (pali). **B** Schematic diagram of **A** showing growth lines (*black lines*). **C** Enlargement of **A**. Growth lines (*dashed lines*) show the extent of vertical and lateral growth. Note that some laterally directed fibrous growth (*s with dotted black line*) cannot be related directly to an EMZ. Hence, that growth could be substantially younger having been deposited any time prior to emplacement of a dissepiment above it

Table 2 Range of published annual extension rates and calculated rates of dissepiment emplacement (calice depth/extension rate) for four common reef building coral genera

Species	Location	Extension rate (mm/year)		Reference	Calice depth/extension rate (days)	
		Min	Max		Min	Max
Acropora spp	Somoa	4.0	185.0	Mayor 1924	547.5	11.8
Acropora cytherea	Solitary Islands	20.9		Harriott 1999	104.8	
Pocillopora damicornis	Panama	6.0	72.0	Glynn and Stewart 1973	73.0	6.1
Goniastrea retiformis	Enewetak	5.0	9.5	Highsmith 1979		238.2
Goniastrea favulus	GBR	3.8	4.3	Babcock 1988	595.5	526.3
Porites spp	GBR	8.8	21.7	Lough and Barnes 1997	91.3	37.0
Porites lobata	Indonesia	11.7	16.3	Edinger et al. 2000	68.6	49.3

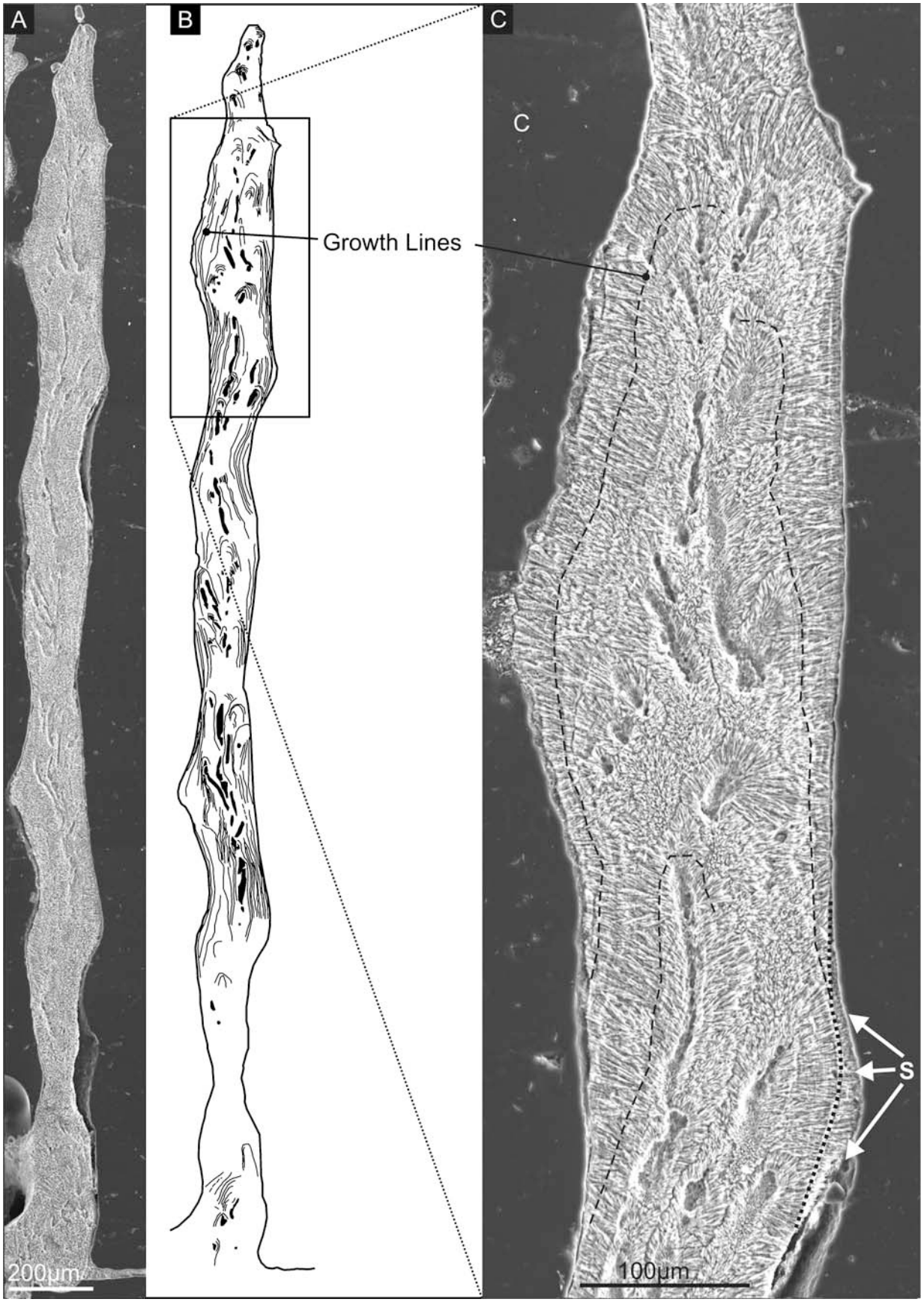
A
B
C
C
Growth Lines
S
200µm
100µm

placement of such patches relative to the underlying fibers is difficult to establish and could represent some degree of temporal disjunction.

Implications for geochemical proxies

For corals to serve as ideal geochemical proxies, their skeletons would accrete along smooth, continuous fronts at a uniform rate in the direction of extension, thus forming layers analogous to tree rings. However, the complex microstructure of the coral skeleton and differential timing of emplacement of different fiber associations (e.g., trabeculae before bundles) are far from ideal. Several studies utilizing scleractinian corals have documented large trace element heterogeneities on scales of less than 100 μm (Allison 1996; Cohen et al. 2001; Marshall and McCulloch 2002; Allison and Finch 2004). These variations are too large to reflect changes in SST, for example, and have been attributed to biological and/or kinetic effects that relate to local spatial and temporal variation in seawater parameters, differing calcification rates of the corals, or various unspecified vital effects (e.g., Cohen et al. 2002; Marshall and McCulloch 2002; Meibom et al. 2003; Allison and Finch 2004; Sinclair 2005). These geochemical discrepancies have been highlighted by recent attempts to resolve fine temporal sequences of paleoclimate data (i.e., subannual) by use of increasingly smaller laser or microprobe spot sizes for sampling. However, the most consistent and repeatable data sets are those that represent larger, time averaged samples. Although finer temporal scales have become possible with high-resolution, high-precision microsampling techniques, this sampling must take the exact temporal relationships between adjacent elements of microstructure into account. Even a slight lateral divergence (e.g., from trabeculae into secondary fibronormal thickening or bundles) may invalidate time series data.

Microsampling techniques commonly used for paleoclimate analysis of corals utilize a range of analytical spot sizes. Ion microprobe samples have commonly ranged between 10 and 80 μm in diameter (e.g., Hart and Cohen 1996; Cohen et al. 2002), and LA-ICP-MS laser spot sizes vary in size and shape, including 100 × 500 μm rectangles, 25 × 600 μm rectangles and 175-μm diameter circles (e.g., Sinclair et al. 1998; Fallon et al. 2002). The depth of analysis is rarely reported. The assumption has been that a linear sequence of samples collected along a structure in the direction of overall skeletal extension will represent a temporal sequence of samples. To test that assumption, we have used two methods to calculate the maximum range in age of closely adjacent sections of coral skeleton. First, we determined the length of time that a given skeletal surface within a calice was available for fiber extension (i.e., active growth) before it was isolated within the corallum by emplacement of a dissepiment above it. Secondly, for *Porites,* which has the simplest trabecular microstructure, we used photomicrograph mosaics to trace individual growth lines within skeletal fibers to compare the magnitude of growth vectors in the direction of calical extension and laterally within walls.

For our first method, we divided calice depth by the average annual extension rate. We defined calice depth as the distance from the outer tip of the calice, which is generally trabecular in microstructure, to the most recently deposited dissepiment, which occurs adjacent to a wall that has reached its maximum thickness. The ratio represents the length of time that skeletal surfaces within an individual calice can potentially grow, because skeletal thickening may occur at the base of the calice at the same time as trabecular growth occurs at the tip of the calice. Thus, this calculation gives the potential maximum difference in age between the center of trabeculae at the center of the walls and the last fibers secreted in the adjacent thickening on their flanks (Fig. 15).

A survey of previously published extension rates (Table 2) established the possible range of maximum and minimum values for genera and/or species analyzed in this study. The wide range of growth rates for *Acropora* results in a significant range of possible time intervals between growth of trabeculae and immediately adjacent thickening deposits (between 11.8 and 547.5 days). Hence, if sample locations within an individual vertical structure, such as a wall, stray from the center of a trabecula to the outermost flank, skeletal age could potentially vary by more than 1 year within a lateral distance of only 30–50 μm. As most laser ablation spot sizes are significantly larger than this, our data suggests that most laser ablation samples may represent significantly time-averaged samples encompassing portions of up to 1 year's skeletal growth. Hence, peak summer and winter temperature extremes in SST would invariably be underestimated. Regardless, most *Acropora* accretes more rapidly, providing a good potential for its use as a subannual paleoclimate proxy. However, in such cases of rapid extension, the overall temporal span that can be analyzed is severely limited, and annual growth bands are difficult to recognize in rapidly growing branching forms. Hence, although *Acropora* has been a prolific reef builder since the Late Oligocene (Wallace 1999) it has not been used extensively for paleoclimate records.

Fig. 17 Comparison of geochemical sampling spot sizes and *Porites lobata* microstructure (sample 04-9-30). **A** Photomosaic of scanning electron photomicrographs of polished and etched surface of a septum showing various common sample sizes for laser ablation (*open rectangles* and *circles* for LA-ICP-MS) and ion microprobe (*solid black circles*) analyses of scleractinian corals. **B** Schematic diagram of **A** showing growth lines (*thin black lines*) and EMZ – *black shaded areas*. Line X–Y represents a vertical growth distance of 384 μm, whereas the temporally equivalent line X–Y' represents 36 μm of lateral growth (a ratio of > 10:1). These two lines terminate at the same growth line and therefore grew over the same time interval (~ 20 bands). If it is assumed that the growth lines represent daily increments, most individual laser samples will reflect more than 1 month's worth of skeletal growth. Ion microprobe spot sizes have greater resolution, but note that where they are located in the lateral thickening deposits they may sample fibers of approximately the same age over vertical distances approaching 300 μm

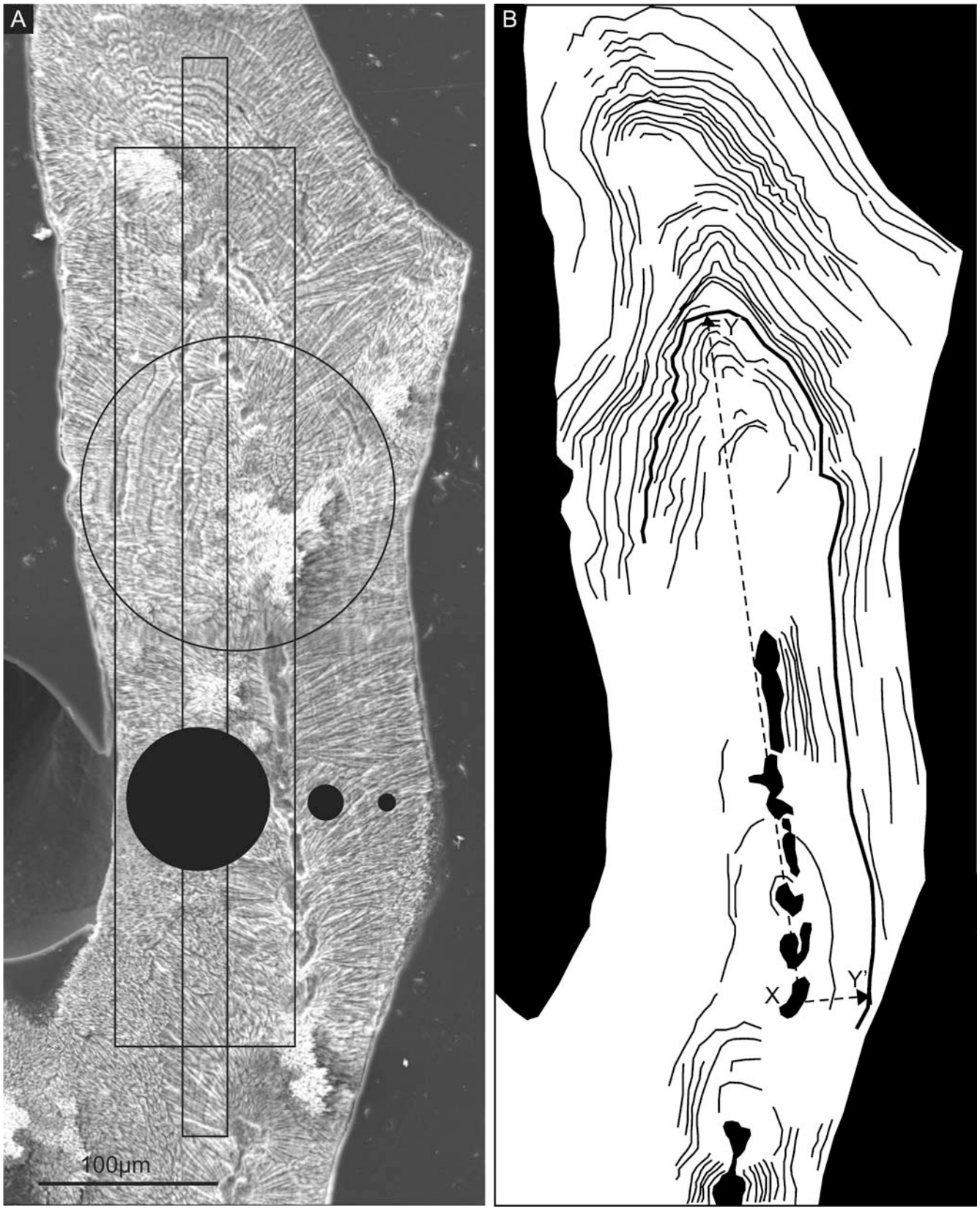
A
100μm
B
Y
X
Y'

Pocillopora also has highly variable extension rates, ranging from 73 to 6.1 days between skeletal growth at the tip and base of the calice. However, *Pocillopora* has a simpler microstructure, with clearly defined septa and limited intra-calice features such as septa and dissepiments, thus allowing for a more continuous temporal sequence of skeletal deposition. Regardless, *Pocillopora* has major problems as a paleoclimate proxy due to the large amount of thickening that occurs at the base of the calice. Such thickening renders it difficult to sample in the direction of extension. The branching habit of corallites also makes recognition of annual bands difficult.

Goniastrea has the potential to serve as a proxy for paleoclimate research because it has a robust septothecal microstructure with clearly defined density bands. However, it and other faviid corals have only rarely been used for environmental analyses (Shen and Boyle 1988; Hanna and Muir 1990; Esslemont 1999; Munksgaard et al. 2004). *Goniastrea* has the slowest extension rate of the corals investigated in this study along with a relatively deep calice. These two factors, together with its relatively complex intra-calical structure, contribute to a large amount of secondary thickening and many temporal disjunctions between skeletal zones within the calice. The result is a large potential time difference between growth at the tip and base of the calice (up to 595.5 days). Even at the highest extension rate recorded for the genus, the difference in depositional time could still be as much as 238.2 days within a lateral distance of only 100–200 μm. Hence, even a small amount of straying towards the outer edge of the wall could represent as much as a 1-year difference in the time of deposition.

Porites is the most commonly used coral genus for environmental analysis because of its easily identified and dateable density bands, the longevity of individual colonies and its widespread global distribution (e.g., Alibert and McCulloch 1997; McGregor and Gagan 2003). Also, as the *Porites* microstructure lacks discrete, secondary thickening phases, such as bundles, there are few obvious temporal disjunctions between adjacent parts of the skeleton. The potential difference between growth of skeleton at the tip and base of the calice ranges from 91.3 to 37 days. This range is similar to that calculated by Barnes and Lough (1993) where they calculated the frequency of dissepiment emplacement, which varies between 107.2 and 30.6 days.

In order to better determine the timing of skeletal emplacement in *Porites*, we applied a second method wherein we traced individual growth layers in fibers through corallite walls on SEM photomicrograph mosaics of polished etched surfaces (Figs. 16, 17). We found that within single continuous vertical growth segments, individual growth layers are traceable for up to 470 μm of vertical growth (Fig. 16C). When this is compared to extension rate data in Table 2, it represents ~10–15 days of growth. Figure 17 shows a vertical section of a septum with easily traced growth lines. Growth lines suggest that 384 μm of vertical growth are equivalent to only 36 μm of lateral growth, measured from the EMZ in the center of the septum to the edge of the growth line. According to global extension rate data in Table 2, the growth increment may represent as many as 12 days of growth. Therefore, as many as 12 days' skeletal growth may represent only 36 μm of skeletal growth. Thus, even a slight stray away from the intended line of sampling in a high-resolution survey may cause data to be missed or resampled within a given time series. If samples are collected in a line parallel, but lateral to the central EMZ, they may fall largely along a single growth line, and many sequential spots may sample skeleton that accreted at the same time. The potential error is much larger in genera such as *Goniastrea* where lateral growth of septa is greater, thus representing larger intervals of time. Owing to differences in microstructure between different genera, direct observation of trabeculae, fibronormal layers and bundles as delineated by etched growth lines may be necessary to allow samples to be placed into series that represent temporal sequences with known degrees of time averaging.

Conclusions

Scleractinian coral genera have varyingly complex microstructures, and no single growth model is adequate to describe coral skeletogenesis. Various types of skeletal infilling and thickening deposits postdate initial wall and septal formation to various degrees, as constrained by the timing of dissepiment emplacement when surfaces are isolated from living tissue and further growth. Hence, immediately adjacent portions of skeleton may have formed at different times of the year, and depending on overall extension rates, calice depth, and rates of dissepiment emplacement; adjacent skeletal accretion may even span seasons or different years. In all cases, current laser and microprobe spot sizes for geochemical sampling involve a degree of time averaging that may also include seasonal overlap. Thus, fine scale geochemical sampling of coral skeletons for high temporal resolution may be distorted where sampling does not take microstructure into account directly. The age of coral skeleton decreases both along trabeculae in the direction of corallum extension and laterally, from the center of trabeculae towards the septal flank within the corallite. The common assumption that a linear sequence of samples collected along a feature in the direction of overall skeletal extension represents a temporal sequence of samples is unfounded in many cases. The variation of microstructures between different genera (particularly the interplay between trabeculae and thickening deposits) becomes especially important where discontinuities are present and represent potentially significant time differences. Thus, a greater understanding of microstructure is required if coral skeletogenesis is be understood adequately for coral skeletons to serve a repositories of temporally constrained geochemical data.

Acknowledgements The authors wish to thank J.E. Sorauf, J.S. Jell, and J.-P. Cuif for discussions on coral microstructure and all staff at the Analytical Electron Microscopy Facility at the Queensland University of Technology (QUT) where all scanning electron microscopy was carried out. We also thank two anonymous reviewers who made very helpful comments on the manuscript. The research was funded by QUT and by a QUT Australian Tertiary Network Small Grant to

Webb. Corals were collected under Marine Parks Permit G03/9787.1 from the Great Barrier Reef Marine Park Authority

References

Alibert C, Kinsley L, Fallon SJ, McCulloch MT, Berkelmans R, McAllister FA (2003) Source of trace element variability in Great Barrier Reef corals affected by the Burdekin flood plumes. Geochim Cosmochim Acta 67:231–246

Alibert C, McCulloch MT (1997) Strontium/calcium ratios in modern *Porites* corals from the Great Barrier Reef as a proxy for sea surface temperature: Calibration of the thermometer and monitoring of ENSO. Paleoceanography 12:345–364

Allison N (1996) Comparative determinations of trace elements in coral aragonite by ion microprobe analysis, with preliminary results from Phucket, southern Thailand. Geochim Cosmochim Acta 60:3457–3470

Allison N, Finch AA (2004) High-resolution Sr/Ca records in modern *Porites lobata* corals: effects of skeletal extension rate and architecture. Geochem Geophys Geosystems 5:Q05001, DOI:10.1029/2004GC000696

Allison N, Tudhope AW (1992) Nature and significance of geochemical variation in coral skeletons as determined by ion microprobe analysis. Proc 7th Int Coral Reef Symp 1:173–178

Babcock RC (1988) Age-structure, survivorship and fecundity in populations of massive corals. Proc 6th Int Coral Reef Symp 2:625–627

Barnes DJ, Lough JM (1993) On the nature and causes of density banding in massive coral skeletons. J Exper Mar Biol Ecol 167:91–108

Beck JW, Edwards RL, Ito E, Taylor FW, Récy J, Rougerie F, Joannot P, Henin C (1992) Sea-surface temperature from coral skeletal strontium/calcium ratios. Science 257:644–647

Bryan WH, Hill D (1941) Spherulitic crystallization as a mechanism of skeletal growth in the hexacorals. Proc Royal Soc Queensland 52:78–91

Cohen AL, Layne GD, Hart SR (2001) Kinetic control of skeletal Sr/Ca in a symbiotic coral: Implications for the paleotemperature proxy. Paleoceanography 16:20–26

Cohen AL, Owens KE, Layne GD, Shimizu N (2002) The effect of algal symbionts on the accuracy of Sr/Ca paleotemperatures from coral. Science 296:331–333

Constantz B, Weiner S (1988) Acidic macromolecules associated with the mineral phase of scleractinian coral skeletons. J Exper Zool 248:253–258

Corrège T (2006) Sea surface temperature and salinity reconstruction from coral geochemical tracers. Palaeogeogr Palaeoclimat Palaeoecol 232:408–428

Cuif J-P, Dauphin Y (1998) Microstructural and physico-chemical characterization of 'centers of calcification' in septa of some Recent scleractinian corals. Paläontol Zeitschrift 72:257–270

Cuif J-P, Dauphin Y (2005) The environmental recording unit in coral skeletons - a synthesis of structural and chemical evidences for a biochemically driven, stepping-growth process in fibres. Biogeosciences 2:67–73

Cuif J-P, Dauphin Y, Berthet P, Jegoudez J (2004) Associated water and organic compounds in coral skeletons: quantitative thermogravimetry coupled to infrared absorption spectrometry. Geochem Geophys Geosyst 5: DOI:10.1029/2004GC000783

Cuif J-P, Dauphin Y, Doucet J, Salome M, Susin J (2003a) XANES mapping of organic sulfate in three scleractinian coral skeletons. Geochim Cosmochim Acta 67:75–83

Cuif J-P, Dauphin Y, Gautret P (1997) Biomineralization features in scleractinian coral skeletons: source of new taxonomic criteria. Boletin Real Sociedad Española Hist Nat, (Seccion Geologia) 92:129–141

Cuif J-P, Lecointre G, Perrin C, Tillier A, Tillier S (2003b) Patterns of septal biomineralization in Scleractinia compared with their 28S rRNA phylogeny: a dual approach for a new taxonomic framework. Zool Scripta 32:459–473

Cuif J-P, Perrin C (1999) Micromorphology and microstructure as expression of Scleractinia skeletogenesis in *Favia fragum* (Esper, 1975) (Faviidai, Scleractinia). Zoosystema 21:137–156

Cuif J-P, Sorauf JE (2001) Biomineralization and diagenesis in the Scleractinia: part 1, biomineralisation. Bull Tohoku Univ Museum 1:144–151

de Villiers S, Nelson BK, Chivas AR (1995) Biological controls on coral Sr/Ca and δ18O reconstructions of sea surface temperature. Science 269:1247–1249

Edinger EN, Limmon GV, Jompa J, Widjatmoko W, Heikoop JM, Risk MJ (2000) Normal coral growth rates on dying reefs: are coral growth rates good indicators of reef health? Mar Pollution Bull 40:404–425

Esslemont G (1999) Heavy metals in corals from Heron Island and Darwin Habour, Australia. Mar Pollution Bull 38:1051–1054

Fallon SJ, McCulloch MT, van Woesik R, Sinclair DJ (1999) Corals at their latitudinal limits: laser ablation trace element systematics in *Porites* from Shirigai Bay, Japan. Earth Planet Sci Lett 172:221–238

Fallon SJ, White JC, McCulloch MT (2002) *Porites* corals as recorders of mining and environmental impacts: Misima Island, Papua New Guinea. Geochim Cosmochim Acta 66:45–62

Gautret P, Cuif J-P, Freiwald A (1997) Composition of soluble mineralizing matrices in zooxanthellate and non-zooxanthellate scleractinian corals: biochemical assessment of photosynthetic metabolism through the study of a skeletal feature. Facies 36:189–194

Gautret P, Cuif J-P, Stolarski J (2000) Organic components of the skeleton of scleractinian corals - evidence from in situ acridine orange staining. Acta Palaeontol Polonica 45:107–118

Gill IP, Dickson JAD, Hubbard DK (2006) Daily banding in corals: Implications for paleoclimatic reconstruction and skeletonization. J Sedim Res 76:683–688

Glynn PW, Stewart RH (1973) Distribution of coral reefs in the Pearl Islands (Gulf of Panama) in relation to thermal conditions. Limnol Oceanogr 18:367–379

Goreau TF (1959) The physiology of skeleton formation in corals. 1. A method for measuring the rate of calcium deposition by corals under different conditions. Biol Bull 116:59–75

Hanna RG, Muir GL (1990) Red Sea corals as biomonitors of trace metal pollution. Environ Monit Assess 14:211–222

Harriott VJ (1999) Coral growth in subtropical eastern Australia. Coral Reefs 18:281–291

Hart SR, Cohen AL (1996) An ion probe study of annual cycles of Sr/Ca and other trace elements in corals. Geochim Cosmochim Acta 60: 3075–3084

Highsmith RC (1979) Coral growth rates and environmental control of density banding. J Experim Mar Biol Ecol 27:105–125

Jell JS (1974) The microstructure of some scleractinian corals. Proc 2nd Coral Reef Symp 2:301–320

Jell JS, Hill D (1974) The microstructure of corals. In: Ancient Cnidaria. Acad Sci. USSR Trans Inst Geol Geophys 201(1):8–14

Johnston IS (1980) The ultrastructure of skeletogenesis in hermatypic corals. Int Rev Cytol 67:171–214

Kato M (1963) Fine skeletal structures in Rugosa. J Faculty Sci Hokkaido Univ 11:571–630

Lafuste J (1970) Lames ultra-minces à faces polies. Procédé et application à la microstructure des Madréporaires fossils. CR Acad Sci Paris 270:679–681

Lafuste J, Plusquellec Y (1985) Structure et microstructure de quelques Micheliniidae et Michelinimorphes (Tabulata paléozoiques). Bull Mus Nat Hist Nat, Paris (4, C) 1:13–63

Lafuste J, Plusquellec Y (1987) Structure et microstructure de *Favosites cylindrica* Michelin 1847, espece-type de *Ohiopora n.* gen. (Tabulata, Devonien). Can J Earth Sci 24:1465–1477

Lafuste J, Plusquellec Y, Soto F (1993) Coexistence de lamelles et de microlamelles dans le sclérenchyme de *"Ligulodictyum"* Plusquellec, 1973 (Tabulata, Dévonien du Nord-Gondwana). Courier Forschungsinstitut Senckenberg 164:329–337

Lea DW, Shen GT, Boyle EA (1989) Coralline barium records temporal variability in equatorial Pacific upwelling. Nature 340:373–376

Linsley BK, Wellington GM, Schrag DP (2000) Decadal sea surface temperature variability in the subtropical South Pacific from 1726 to 1997 A.D. Science 290:1145–1148

Lough JM, Barnes DJ (1997) Centuries-long records of coral growth on the Great Barrier Reef. Great Barrier Reef Marine Park Authority Workshop Series 17:149–157

Marshall AT (2002) Occurrence, distribution, and localisation of metals in cnidarians. Microscopy Res Tech 56:341–357

Marshall JF, McCulloch MT (2002) An assessment of the Sr/Ca ratio in shallow water hermatypic corals as a proxy for sea surface temperature. Geochim Cosmochim Acta 66:3263–3280

Mayor A (1924) Growth rate of Samoan corals. Carnegie Inst Wash Publ 340:51–72

McCulloch MT, Fallon SJ, Wyndham T, Hendy E, Lough JM, Barnes DJ (2003) Coral record of increased sediment flux to the inner Great Barrier Reef since European settlement. Nature 421:727–730

McGregor HV, Gagan MK (2003) Diagenesis and geochemistry of *Porites* coral from Papua New Guinea: implications for paleoclimate reconstruction. Geochim Cosmochim Acta 67:2147–2156

Meibom A, Cuif J-P, Hillion F, Constantz BR, Juillet-Leclerc, Dauphin Y, Watanabe T, Dunbar RB (2004) Distribution of magnesium in coral skeleton. Geophys Res Lett 31:L23306, DOI:10.1029/2004GL021313

Meibom A, Stage M, Wooden J, Constantz BR, Dunbar RB, Owen A, Grumet N, Bacon CR, Chamberlain CP (2003) Monthly strontium/calcium oscillations in symbiotic coral aragonite: biological effects limiting the precision of the paleotemperature proxy. Geophys Res Lett 30:1418–1421

Meibom A, Yurimoto H, Cuif J-P, Domart-Coulon I, Houlbreque F, Constantz B, Dauphin Y, Tambutté E, Tambutté S, Allemand D, Wooden J, Dunbar R (2006) Vital effects on coral skeletal composition display strict three-dimensional control. Geophys Res Lett 33:L11608, DOI:10.1029/2006GL025968

Mitterer RM (1978) Aminoacid composition and metal binding capability of the skeletal proteins of coral. Bull Mar Sci 28:173–180

Munksgaard NC, Antwertinger Y, Parry DL (2004) Laser Ablation ICP-MS analysis of Faviidae corals for environmental monitoring of tropical estuary. Environ Chem 1:188–196

Nothdurft LD, Webb GE (in press) 'Shingle' microstructure in scleractinian corals: a possible analogue for lamellar and microlamellar microstructure in Palaeozoic tabulate corals. Schriftenreihe der Erdwissenschaftlichen Kommissionen

Oekentorp KAW (2001) Review on diagenetic microstructures in fossil corals - a controversial discussion. Bull Tohoku Univ Mus 1:193–209

Ogilvie MM (1896) Microscopic and systematics study of madreporarian types of corals. Phil Trans Roy Soc Lond 29:83–345

Perrin C (2003) Compositional heterogeneity and microstructural diversity of coral skeletons: implications for taxonomy and control on early diagenesis. Coral Reefs 22:109–120

Perrin C (2004) Diagenese precoce des biocristaux carbonayes: tranformations isominerales de l'aragonite corallienne. Bull. Soc. Geol. France 175:95–106

Perrin C, Cuif J-P (2001) Ultrastructural controls on diagenetic patterns of scleractinian skeletons: evidence at the scale of colony lifetime. Bull Tohoku Univ Mus 1:210–218

Rodriquez S (1989) Lamellar microstructure in Palaeozoic corals: origin and use in taxonomy. Mem Assoc Australas Palaeontols 8:157–168

Rollion-Bard C, Blamart D, Cuif J-P, Juillet-Leclerc A (2003) Microanalysis of C and O isotopes of azooxanthellate and zooxanthellate corals by ion microprobe. Coral Reefs 22:405–415

Roniewicz E (1996) The key role of skeletal microstructure in recognizing high-rank scleractinian taxa in the stratigraphical record. Paleontol Soc Papers 1:187–206

Runnalls LA, Coleman ML (2003) Record of natural and anthropogenic changes in reef environments (Barbados West Indies) using laser ablation ICP-MS and sclerochronolgy on coral cores. Coral Reefs 22:416–426

Semenoff-tian-Chansky P (1984) Microstructure of *Siphonodendron* (Lithostrotionidae). Palaeontogr Amer 54:489–500

Shen GT, Boyle EA (1988) Determination of lead, cadmium and other trace metals in annually-banded corals. Chem Geol 67:47–62

Sinclair DJ (2005) Correlated trace element "vital effects" in tropical corals: a new geochemical tool for probing biomineralization. Geochim Cosmochim Acta 69:3265–3284

Sinclair DJ, Kinsley LPJ, McCulloch MT (1998) High-resolution analysis of trace elements in corals by laser ablation ICP-MS. Geochim Cosmochim Acta 62:1889–1901

Sinclair DJ, McCulloch MT (2004) Corals record low mobile barium concentrations in the Burdekin River during the 1974 flood: evidence for limited Ba supply to rivers? Palaeogeogr Palaeoclimat Palaeoecol 214:155–174

Sorauf JE (1970) Microstructure and formation of dissepiments in the skeleton of recent Scleractinia (hexacorals). Biomineralization 2:1–22

Sorauf JE (1972) Skeletal microstructure and microarchitecture in Scleractinia (Coelenterata). Palaeontol 15:88–107

Sorauf JE (1993) The coral skeleton: analogy and comparisons, Scleractinia, Rugosa, and Tabulata. Courier Forschungsinstitut Senckenberg 164:63–70

Sorauf JE (1996) Biocrystallization models and skeletal structure of Phanerozoic corals. Paleontol Soc Papers 1:159–185

Sorauf JE, Podoff N (1977) Skeletal structure in deep water ahermatypic corals. Mém Bur Rech Géol Minièr 89:2–11

Stolarski J (2003) Three-dimensional micro- and nanostructural characteristics of the scleractinian coral skeleton: a biocalcification proxy. Acta Palaeontol Polonica 48:497–530

Stolarski J, Mazur M (2005) Nanostructure of biogenic versus abiogenic calcium carbonate crystals. Acta Palaeontol Polonica 50:847–865

Towe KM (1972) Invertebrate shell structure and the organic matrix concept. Biomineralization 4:1–7

Vandermeulen JH, Watabe N (1973) Studies on reef corals. I. Skeleton formation by newly settled planula larva of *Pocillopora damicornis*. Mar Biol 23:47–57

Veron JEN (1986) Corals of Australia and the Indo-Pacific. Angus and Robertson Publishers, Australia, 644 pp

Wallace CC (1999) Staghorn corals of the world: a revision of the coral genus Acropora. CSIRO Publishing, Collingwood, 421 pp

Wang HC (1950) A revision of the Zoantharia Rugosa in the light of their minute skeletal structures. Phil Trans R Soc Lond B 234:175–246

Wise SWJ (1970) Scleractinian coral exoskeletons: surface microarchitecture and attachment scar patterns. Science 169:978–980

Wyndham T, McCulloch M, Fallon S, Alibert C (2004) High-resolution coral records of rare-earth elements in coastal seawater: biogeochemical cycling and a new environmental proxy. Geochim Cosmochim Acta 68:2067–2080